A Reproduced Copy

DRA/LANGLEY

OLD DOMINION UNIVERSITY RESEARCH FOUNDATION

DEPARTMENT OF MECHANICAL ENGINEERING AND MECH...
SCHOOL OF ENGINEERING
OLD DOMINION UNIVERSITY
NORFOLK, VIRGINIA

FINITE ELEMENT THERMAL-STRUCTURAL ANALYSIS OF CABLE-STIFFENED SPACE STRUCTURES

By

Earl A. Thornton, Principal Investigator

Pramote Dechaumphai, Research Associate

and

Ajay K. Pandey, Graduate Research Assistant

Final Report
For the period ending February 1, 1984

Prepared for the
National Aeronautics and Space Administration
Langley Research Center
Hampton, Virginia

Under
Research Grant NAG-1-257
Dr. L. Bernard Garrett, Technical Monitor
SSD-Systems & Experiments Branch

April 1984

DEPARTMENT OF MECHANICAL ENGINEERING AND MECHANICS
SCHOOL OF ENGINEERING
OLD DOMINION UNIVERSITY
NORFOLK, VIRGINIA

FINITE ELEMENT THERMAL-STRUCTURAL ANALYSIS OF CABLE-STIFFENED SPACE STRUCTURES

By

Earl A. Thornton, Principal Investigator

Pramote Dechaumphai, Research Associate

and

Ajay K. Pandey, Graduate Research Assistant

Final Report
For the period ending February 1, 1984

Prepared for the
National Aeronautics and Space Administration
Langley Research Center
Hampton, Virginia

Under
Research Grant NAG-1-257
Dr. L. Bernard Garrett, Technical Monitor
SSD-Systems & Experiments Branch

Submitted by the
Old Dominion University Research Foundation
P. O. Box 6369
Norfolk, Virginia 23508

April 1984

ABSTRACT

FINITE ELEMENT THERMAL-STRUCTURAL ANALYSIS OF
CABLE-STIFFENED SPACE STRUCTURES

Finite element thermal-structural analyses of cable-stiffened space structures are presented. A computational scheme for calculation of prestresses in the cable-stiffened structures is also described. The determination of thermal loads on orbiting space structures due to environmental heating is described briefly. Three finite element structural analysis techniques are presented for the analysis of prestressed structures. Linear, stress stiffening and large displacement analysis techniques are investigated.

The three techniques are employed for analysis of prestressed cable structures at different prestress levels. The analyses produce similar results at small prestress but at higher prestress differences between the results become significant. For the cable-stiffened structures studied, the linear analysis technique may not provide acceptable results. The stress stiffening analysis technique may yield results of acceptable accuracy depending on the prestress. The large displacement analysis technique produces accurate results over a wide range of prestress and is recommended as a general analysis technique for thermal-structural analysis of cable-stiffened space structures.

TABLE OF CONTENTS

TABLE OF CONTENTS - Continued

TABLE OF CONTENTS - Concluded

LIST OF TABLES

LIST OF FIGURES

LIST OF FIGURES - Concluded

LIST OF SYMBOLS

a_s	Surface absorbtivity for solar radiation
a_e	Surface absorbtivity for earth radiation
A	Cross-sectional area
A_F	Solar albedo factor
A_q	Incident heating area
A_r	Element radiation area
[B]	Matrix containing direction cosines of structural member
[BM]	Modified form of [B] matrix after imposing known member forces
c	Specific heat
d	Diameter
e	Axial strain
E	Modulus of elasticity
F	View factor
F_x, F_y, F_z	Member force components in Cartesian coordinates
{F}	Unknown member force vector
$\{F\}_{\varepsilon_0}$	Finite element force vector due to thermal strain
$\{F\}_{\sigma_0}$	Finite element force vector due to prestress
g	Acceleration due to gravity
H	Horizontal component of force in cable
j	Total number of equations for prestress analysis
[J]	Finite element Jacobian matrix
k	Thermal conductivity, spring constant

$[K]$	Finite element stiffness matrix
ℓ	Length
L	Finite element length
m	Mass, iteration number
$\{P\}$	Unknown member force vector
P_1	Force on node 1
P_2	Force on node 2
q	Total incident heat load
q_a	Earth reflected solar heating
q_e	Earth emitted heating
q_s	Incident solar heating
$\{R\}$	Residual load vector
S	Cable length
T	Element temperature
T_i	Initial element temperature
u_1, u_2	Local x-displacement components
U	Elastic strain energy
$\{u\}$	Unknown nodal displacement vector
$\{\Delta u\}$	Unknown nodal displacement increment vector
v_1, v_2	Local y-displacement components
V	Volume, potential energy due to external loads
w_1, w_2	Local z-displacement components
w	Global z-displacement component
x, y, z	Cartesian coordinates
α	Coefficient of thermal expansion, orbital position

LIST OF SYMBOLS - Concluded

ϵ	Total strain
ϵ_0	Thermal strain
θ	Element rotation in local x-y plane
π	Total potential energy
ρ	Density
σ	Element stress
σ_0	Element prestress
ψ	Element rotation in local x-z plane

Chapter 1

INTRODUCTION

1.1 Background

Past and proposed future flights of space shuttles have brought the world into the era of space transportation. In the near future, large space structures will be placed in earth orbits. Two basic classes of orbiting large space structures proposed for communications, earth observation and remote sensing are large antennas and space platforms. Figure 1, [1]*, shows an artist's depiction of a large antenna in earth orbit.

To assure satisfactory performance of orbiting structures, analyses of structural integrity and stability are required. These analyses include prediction of structural deformations introduced by cyclic heating on the structure during the orbit. The deformations must be kept within design allowable tolerances to assure satisfactory structural performance. Due to the large size of these structures, ground testing is not possible, and thus reliable analyses are required to predict structural deformations accurately.

To increase the structural stability and to provide additional stiffness to the structural system, the concept of prestressed,

*The numbers in brackets indicate references.

Fig. 1 An artist's depiction of a large antenna in earth orbit [1].

cables and membranes have been proposed for some designs [1-3]. Prestressed structures, such as the hoop column antenna, shown in Fig. 2, [1], can provide ease of deployment while maintaining low mass and stability. Cable-stiffened space structures are difficult to analyze because: (1) all members have prestresses, (2) cables cannot take compressive forces, and (3) large deformations may be experienced. For large structures with cables, it is possible that displacements may be large due to on-orbit loads. This introduces nonlinear effects which should be considered for the structural analysis to predict deformations accurately.

Prediction of structural deformations depends primarily on the accuracy of the heating, thermal and structural analyses techniques adopted. Finite element methods are used extensively for such thermal and structural problems [4]. Finite element methods are used extensively for linear type structural analysis with codes such as NASTRAN and ANSYS. These codes have limited capability for structural analysis of cable-stiffened structures with member prestress. The ANSYS finite element structural analysis program uses a "stress-stiffening technique" for prestressed structures. Many existing finite element codes do not have capability for the determination of prestress for the structural analysis of cable-stiffened structures.

1.2 Literature Review

To predict the displacements caused by on-orbit heat loads, three steps are required: (1) calculation of heat loads, (2) calculation of

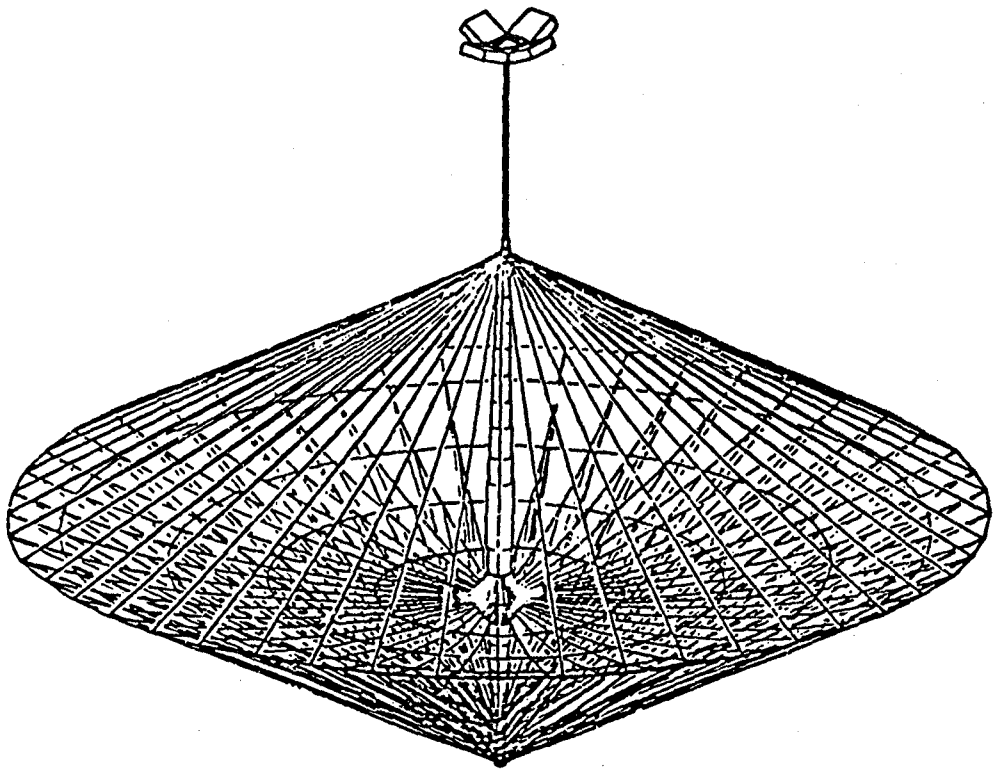

Fig. 2 A cable-stiffened hoop column antenna [1].

temperatures, and (3) calculation of displacements and stresses due to the temperature distribution in the structure. These tasks have been the subject of recent research.

Mahaney and Strode [5] present a clear description of the heat load calculation on orbiting structures. The calculation of structural temperatures at different points in the orbit is a transient problem often based on simplifying assumptions. Arduini [6] presents a discussion of the accuracy of thermal analyses by citing uncertainties in calculation of view factors, member to member shadowing, member to member radiation exchange, and conductivity calculation of composite materials. Chambers, Jensen and Coyner [7] describe a thermal analysis approach consisting of the MIDAS/TRASYS programs in which solar shadowing including umbra-penumbra effects and circumferential gradients in element temperatures are considered.

Thermal-structural analysis of space structures without prestresses in members has been discussed in many papers. Reference [8] presents an integrated finite element thermal structural analysis technique to predict deformation and stresses. In reference [5] a tetrahedral truss has been analyzed for on-orbit heating, and it has been shown that deformation of the structure is significant. Bowles and Tenney [9] discuss the thermal expansion of the composite materials proposed for large space structures and show that thermal loads have significant effects on the structural deformation.

Cables are proposed for many space structures including the Hoop Column Antenna [1], Stayed Column [2], Mechanically Scanned Deployable

Antenna (MSDA) [3], Cable Boom System [10], Lunar Anchored Satellite [11], Geosynchronous Tidal Web [12], and Space Elevators [13]. Structural analyses of some of the above space structures that have pretensioned cable elements have been presented in references [1, 3]. Thermal-structural analysis of the MSDA [3] is performed using NASTRAN, and ANSYS is used for analysis of the antenna mesh using the stress stiffening technique. The effect of prestresses in the structure on the structural analysis has not been investigated.

Conaway [14] presents a comparison between linear and geometrically nonlinear finite element structural analysis of some simple structures and shows that nonlinear behavior should be taken into consideration in structural analysis.

Classical cable structures are considered in a book by Irvine [15]. Analytical solutions of cable structures are given including deflection of a catenary due to thermal loading. Baron and Venkatesan [16] present analyses of geometrically nonlinear structures composed of elastic members capable of resisting axial forces only. Cable prestresses have not been included in this analysis. Cable-stiffened space structures are different from classical cable structures because: (1) gravity loads are negligible in space, (2) they have negligible mechanical loads, and (3) cables have pretensions.

1.3 Objectives

The literature review has indicated that little information is available on the thermal-structural behavior of orbiting prestressed

structures. The present work concentrates on the investigation of three finite element structural analysis techniques and the effect of prestress on the accuracy of the techniques. To predict the structural deformations of cable-stiffened structures and to compare the different structural analysis techniques, the following specific objectives are considered:

1. Development of a computational technique to perform the prestress analysis of a space structure,
2. Development of alternative thermal-structural analysis techniques for cable-stiffened orbiting space structures, and
3. Evaluation and identification of the most suitable analysis for cable-stiffened large space structures.

To meet the objectives mentioned above, finite element methods are used to perform the various analyses. Chapter 2 describes heating and thermal analyses. The prestress analysis is presented in Chapter 3. Chapters 4, 5, and 6 describe three approaches for performing the thermal-structural analysis for cable-stiffened structures. Chapter 7 verifies the structural analyses techniques by analyzing two simple problems for which analytical solutions are known. Typical results of thermal-structural analysis of a two-dimensional pretensioned cable system and three-dimensional hoop column antenna are presented in Chapter 8. Based on these analyses, the three structural analyses techniques are discussed and evaluated. Appendices A and B contain finite element matrices for the two nonlinear structural analysis techniques.

Chapter 2

HEATING AND THERMAL ANALYSES

During orbit, structural deformations and thermal stresses are produced due to environmental heating. To perform the structural analysis, the structural temperature distribution is needed to compute the thermally equivalent nodal forces. The structural temperature distribution can be computed if the environmental heating is known. The computational approach used for heating and thermal analyses are explained in this chapter. The computational approach is highlighted herein, further details are presented in [5].

2.1 Heating Analysis

The environmental heat sources applied to the space structure are solar heating, earth emitted heating and earth reflected solar heating. Earth emitted heating and earth reflected solar heating depend on altitude and orientation of the structure. The total incident heat load q (per unit area) on the structure is given by

$$q = q_s + q_e + q_a \tag{2.1}$$

where q_s, q_e and q_a are the incident solar heating, incident earth emitted heating and earth reflected solar heating, respectively.

The incident solar heating q_s, is given by the product of the solar flux, surface absorbtivity for solar radiation (a_s) and cosine of angle (ψ) between the solar flux vector and the structure surface normal as follows:

$$q_s = 1390\ (W/m^2)\ a_s \cos\psi. \qquad (2.2)$$

The earth emitted heating q_e is a function of the Stefan-Boltzmann constant (σ), surface absorbtivity for earth radiation (a_e), a view factor (F) and the temperature of the earth (T_e), which is assumed to be constant at 289K:

$$q_e = \sigma\ a_e\ F\ T_e^4. \qquad (2.3)$$

The view factor F is defined as the fraction of total radiant energy leaving the earth that arrives at the structural surface.

The earth reflected solar heating q_a depends on the solar flux in earth orbit, solar albedo factor (AF), a view factor (F), the surface absorbtivity for solar radiation (a_s) and orientation angle (θ):

$$q_a = 1390\ (W/m^2)\ AF \cos\theta\ a_s\ F. \qquad (2.4)$$

The solar albedo factor is defined as the fraction of solar radiation striking the earth that is reflected back into space.

If the structure enters the earth's shadow during the orbit, the heating on the structure is greatly reduced due to the absence of solar

heating. The duration of the shadowing depends upon the altitude of the orbit. Although the shadow portion of the orbit has two regions, namely, umbra and penumbra, the transit time through the penumbra is very small and can be neglected. The present study uses a geosynchronous orbit (GEO) which has an altitude of 42000 km. The heating on a member depends strongly on a member's orientation with respect to the solar vector and, consequently, may vary significantly from member to member and with time during the orbit. The calculation of the structural heat load is performed at different orbital positions which may be specified. The results are used for the structural thermal analysis described in the following section.

2.2 Thermal Analysis

Once the heat load on the structural member has been determined, the structural temperature distribution at different orbital positions can be computed. Basic types of heat transfer for a typical space structure element are member conduction and surface radiation. The heat transfer problem also involves member to member heat radiation exchanges, shadowing of one member by another and temperature gradients along the length, through the thickness and around the circumference of a member. Member to member radiation exchanges are negligible [5] compared to incident and emitted radiation, so they are disregarded. Shadowing of one member by other members is very complicated and expensive. It has not been determined if a detailed shadowing analysis is necessary to predict structural deformations accurately. For the current studies,

member to member shadowing will be disregarded. For simplicity, temperature gradients through the thickness of a member will be disregarded. This latter assumption is a very good approximation for the thin cables of graphite epoxy considered in this study.

With these assumptions the governing differential equation for a structural member is

$$\rho\, c\, V \frac{\partial T}{\partial t} + \sigma\, \epsilon\, A_r\, T^4 - \frac{\partial}{\partial x}\left[kA\, \frac{\partial T}{\partial x}\right] = a_s\, A_q\, q(t) \qquad (2.5)$$

where the terms on the left hand side of the equation represent energy stored in the member by thermal capacitance and the temperature change of element with respect to time, the energy emitted due to radiation and heat transfer due to conduction. The right hand side term is the incident heat load, which is a funtion of time. In the above equation ρ is density, c is specific heat, V is the member volume, σ is the Stefan-Boltzmann constant, ϵ is surface emissivity, A_r is the element radiation area, k is the thermal conductivity, and A is the member cross sectional area. On the right hand side a_s is the surface absorbtivity, A_q is the incident heating area, and $q(t)$ is the incident heating rate per unit area.

For a structure made from composite materials such as graphite epoxy, heat transfer from one member to another by conduction is small compared to structures made of metallic members such as aluminum due to the low thermal conductivity of composite materials. Thus for composite

materials the temperature is nearly uniform along the element length. For this case Eq. (2.5) reduces to:

$$\rho\ c\ V \frac{\partial T}{\partial t} + \sigma\ \varepsilon\ A_r\ T^4 = a_s\ A_q\ q(t) \qquad (2.6)$$

This differential equation is used to formulate an isothermal finite element. With this concept, element temperatures for each member can be computed independently. A typical equation is solved using the Crank-Nicholson finite difference technique for transient time marching and Newton-Raphson iteration at each time step. The temperature distribution of the structure may be determined at each time step for the entire orbit in this manner.

Chapter 3

PRESTRESS ANALYSIS

Many proposed large space structures use prestressed elements such as cables and rods to provide stiffness and stability of the structural system. Reference [1] presents details of a cable stiffened hoop column antenna. For such structures before performing a structural analysis, a prestress analysis is required to determine the tensile (or compressive) forces and stresses in each member. The basic requirements for the prestress analysis are that the structure: (1) maintain the required geometry, and (2) be in static equilibrium. This chapter describes the theoretical development for the prestress analysis used in this study and presents an example of a simple analysis.

3.1 Theoretical Development

For a given geometry, the equilibrium equations for a truss-type structure at each joint are:

$$\Sigma F_x = 0$$
$$\Sigma F_y = 0$$
$$\Sigma F_z = 0$$

where F_x, F_y and F_z are member force components in Cartesian

coordinates. For a structure with n joints there are, therefore, 3n equilibrium equations for the entire structure. For a truss-type structure with m members, there are m unknown member forces, F_i, i = 1, 2,..m, and the above equations can be written in matrix form as:

$$\begin{bmatrix} B_{11} & B_{12} & \cdot & \cdot & \cdot & B_{1m} \\ B_{21} & B_{22} & \cdot & \cdot & \cdot & B_{2m} \\ \cdot & \cdot & \cdot & \cdot & \cdot & \cdot \\ \cdot & \cdot & \cdot & \cdot & \cdot & \cdot \\ \cdot & & \cdot & \cdot & \cdot & \cdot \\ B_{(3n)1} & B_{(3n)1} & \cdot & \cdot & \cdot & B_{(3n)m} \end{bmatrix} \begin{Bmatrix} F_1 \\ F_2 \\ \cdot \\ \cdot \\ \cdot \\ F_m \end{Bmatrix} = \begin{Bmatrix} 0 \\ 0 \\ 0 \\ \cdot \\ \cdot \\ 0 \end{Bmatrix}$$

(3n * m) (m*1) (3n*1)

or

$$[B]\{F\} = \{0\} \qquad (3.1)$$

In the above equation, [B] contains direction cosines of the members, and {F} in an unknown vector which contains element forces. The right-hand side vector is a null vector.

Since some of the member forces are specified, the corresponding columns in [B] matrix are multiplied by the specified forces and transferred to the right-hand side of the equation. Depending on the total number of equations and total number of unknown member forces, either additional forces are specified, or extra equations are discarded to provide the number of equations equal to the number of unknowns. In implementing this approach in the computer program, the equilibrium equations are not written at fixed joints. For some structures, if equations are written at all free joints then the number of equations

becomes more than the number of unknowns. For such problems, additional joints are fixed in order to provide the number of equations equal to the number of unknowns. If the total number of unknown member forces is more than the total number of equations then additional member forces need to be specified. This results in the following matrix equation:

$$\underset{jxj}{[BM]}\ \underset{jx1}{\{P\}} = \underset{jx1}{\{R\}} \qquad (3.2)$$

where j is the total number of unknown member forces to be determined. $[BM]$ is the modified form of the $[B]$ matrix after imposing the known member forces, $\{P\}$ is the unknown member force vector, and $\{R\}$ is the load vector. Equation (3.2) is a linear set of simultaneous equations that can be solved directly for the unknown member forces.

The number of unknowns shown in Eq. (3.2) can be reduced if the structure has geometric symmetry. In this case, both members and nodes which are symmetric are first identified. The symmetrical elements produce identical member forces and the symmetrical nodes generate identical equations. The use of symmetry reduces the number of equations to be solved.

An analysis of a structure with symmetry is performed by grouping all identical members in one element group. This reduces the total number of element groups. Similarly, the symmetrical nodes, which generate identical equations, are grouped in one nodal group. Equilibrium equations are written for each nodal group.

The final linear simultaneous equations which contain forces for

different element groups can then be solved using the procedures previously described. Equation (3.1) is written where the size of [B] is given by (3 * nodal group)* (element group); and {F} is a vector containing the total number of element group forces. To clarify these procedures an example of a prestress analysis for a symmetrical structure is presented in the next section.

3.2 Example

Figure 3 shows a planar two-dimensional structure with six nodes and five members. Nodes 1, 2, 5 and 6 are fixed where nodes 3 and 4 are free. Symmetry may be used in solving for the member forces. To maintain the structure in the geometry shown, the forces in members 1 and 5 are identical and similar with the forces in members 2 and 4. Members 1 and 5 are grouped in element group two. Member 3 is placed in element group three. Nodes 3 and 4 which are free nodes generate identical equations. Thus nodes 3 and 4 are kept in nodal group one. Nodes 1, 2, 5 and 6 are grouped in nodal group two. At this point, there are two equations corresponding to nodal group one, and three unknowns corresponding to each element group.

The equilibrium equations obtained from node 3 from nodal group one are,

$$-F_1 \cos\theta_1 + F_2 \cos\theta_2 + F_3 \cos 90^\circ = 0$$

and

$$F_1 \sin\theta_1 + F_2 \sin\theta_2 - F_3 \sin 90^\circ = 0$$

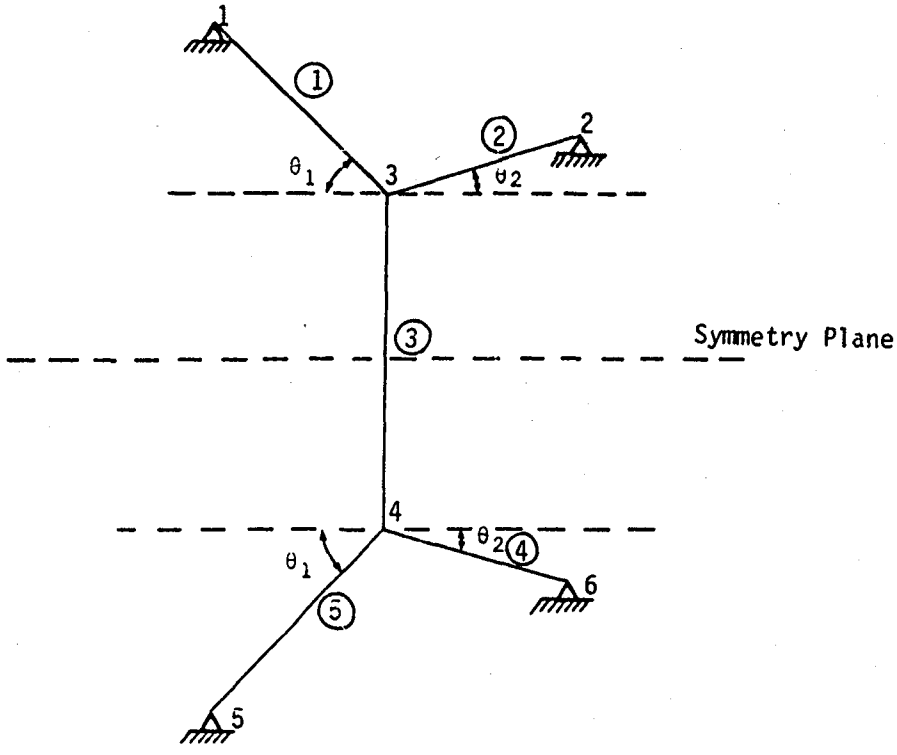

Fig. 3 A two-dimensional symmetric structure for prestress analysis.

where F_1, F_2, F_3 are forces for element groups 1, 2 and 3 respectively. These can be written in matrix form as,

$$\begin{bmatrix} -\cos\theta_1 & \cos\theta_2 & 0 \\ \sin\theta_1 & \sin\theta_2 & -1 \end{bmatrix} \begin{Bmatrix} F_1 \\ F_2 \\ F_3 \end{Bmatrix} = \begin{Bmatrix} 0 \\ 0 \end{Bmatrix}$$

If F_3 is specified then the above matrix equation reduces to,

$$\begin{bmatrix} -\cos\theta_1 & \cos\theta_2 \\ \sin\theta_1 & \sin\theta_2 \end{bmatrix} \begin{Bmatrix} F_1 \\ F_2 \end{Bmatrix} = \begin{Bmatrix} 0 \\ F_3 \end{Bmatrix}$$

With two equations, the unknowns forces F_1 and F_2 for element groups 1 and 2 can be solved. Therefore, all the element forces can be obtained. Once the forces in each member have been determined, the stresses are computed.

Figure 4 shows a flowchart of the prestress analysis program. Nodal coordinates, element connections and symmetry data are read first. The program calculates the total number of unknowns and total number of equations. If the specified forces are not sufficient, the program prints a message in the output file and stops. Equation (3.2) is formulated directly and unknown forces are solved. The program calculates and writes the member stresses on the output file, which are used for the structural analysis as member prestresses.

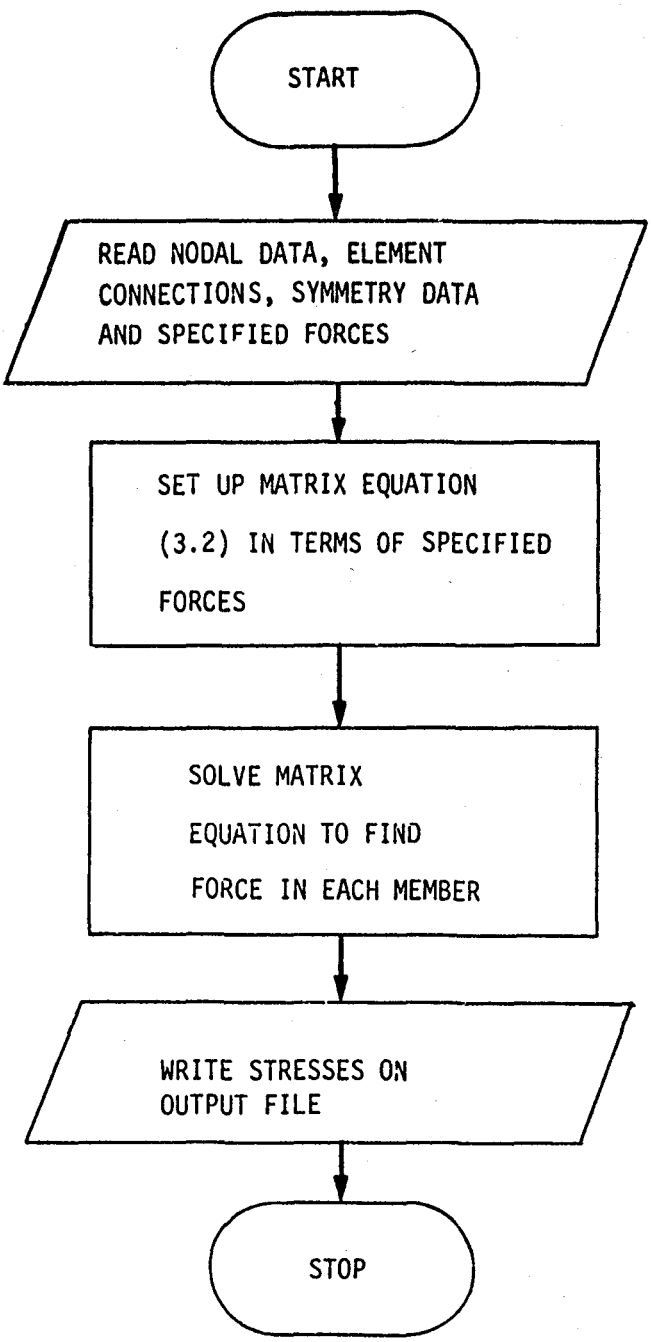

Fig. 4 Flowchart of the prestress analysis program.

Chapter 4

SMALL DEFLECTION STRUCTURAL ANALYSIS

The objectives of the structural analysis are to predict deformations and stresses for the structure during the orbit. The methods for calculating the thermal loads on the structure and prestresses in different members are given in Chapters 2 and 3. Figure 5 shows the thermal-structural analysis procedure for prestressed structures. In this chapter small deflection structural analysis using the finite element method is described.

4.1 Theory

To derive the structural finite element equations for a one-dimensional rod or cable element, a variational principle is employed [4]. Basic equations required to derive finite element equations are explained in this section.

4.1.1 Stress-Strain Relation

The stress-strain relation for a member with prestress and thermal strain is shown in Fig. 6 and is given by,

$$\sigma = E (\varepsilon - \varepsilon_0) + \sigma_0 \qquad (4.1)$$

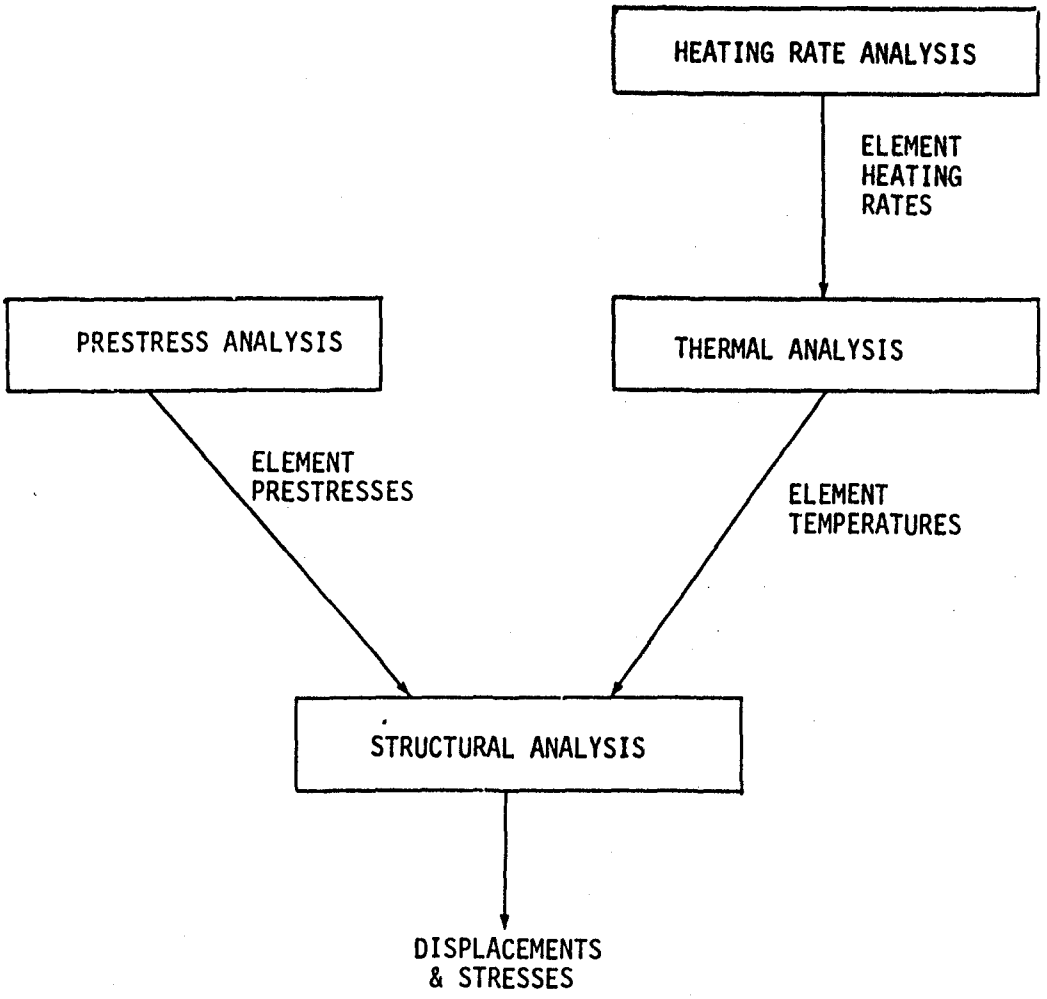

Fig. 5 Thermal-structural analysis procedure.

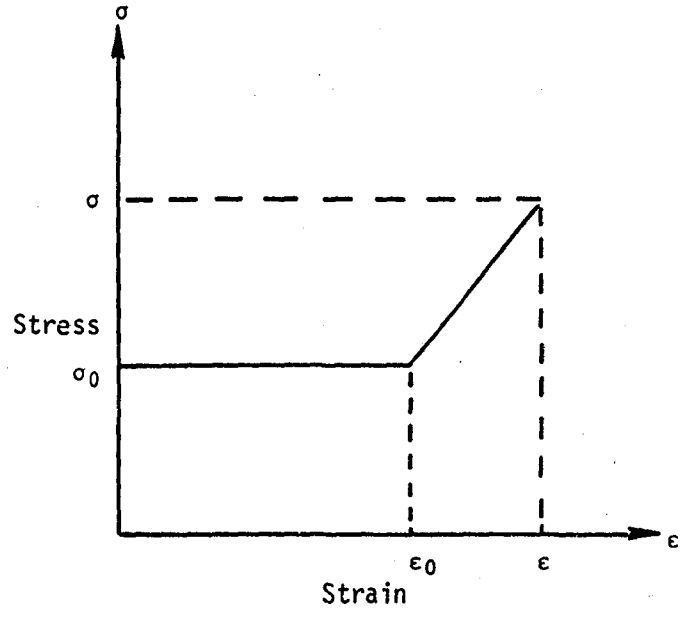

Fig. 6 Stress-strain relation with prestress and prestrain for an one-dimensional element.

where σ is the element stress, E is the modulus of elasticity, ε is the total strain, ε_0 is the thermal strain and σ_0 is the element prestress.

4.1.2 Elastic Strain Energy

The elastic strain energy of the element is given by the integral of the area under the stress-strain curve over the volume of an element,

$$U = \frac{1}{2} \int_{\bullet}^{L} A(\sigma-\sigma_0)\ (\varepsilon-\varepsilon_0)\ dx + \int_{\bullet}^{L} A\ \sigma_0\ \varepsilon\ dx$$

where A is the cross-sectional area and L is the element length. Using the stress-strain relation, Eq. (4.1), the strain energy becomes,

$$U = \frac{AE}{2} \int_{\bullet}^{L} (\varepsilon^2+\varepsilon_0^2 - 2\ \varepsilon\ \varepsilon_0)\ dx + A \int_{\bullet}^{L} \sigma_0\ \varepsilon dx \qquad (4.2)$$

4.1.3 Strain-Displacement Relation

Figure 7 shows a one-dimensional rod or cable element in Cartesian global XYZ coordinates. The element lies on the local X axis. For small deflection theory, the strain-displacement relation is given by,

$$\varepsilon = \frac{\partial u}{\partial x} = \frac{u_2 - u_1}{L} \qquad (4.3)$$

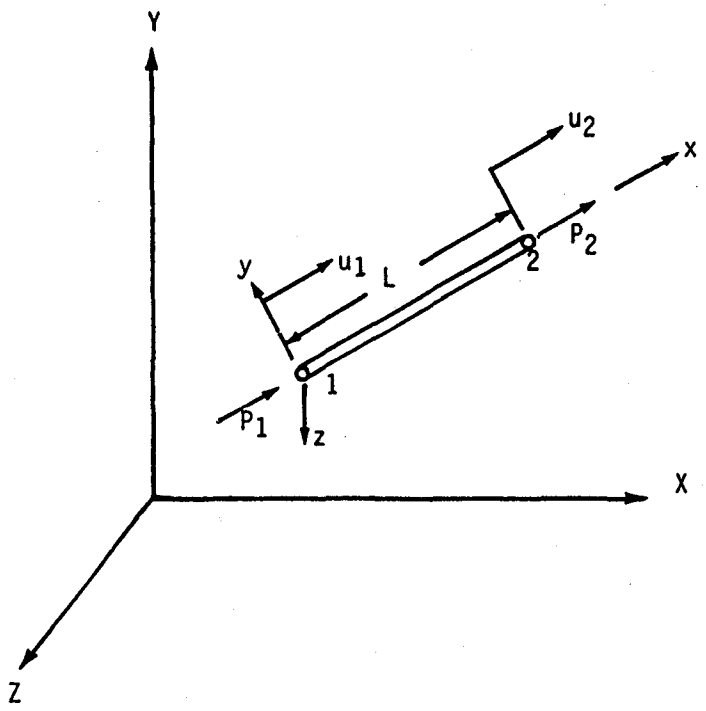

Fig. 7 One-dimensional finite element in local and global coordinates.

where u_1, u_2 are the element nodal displacements in local coordinates.

4.2 Element Equations

4.2.1 Element Potential Energy

The potential energy is the sum of the elastic strain energy and potential energy due to external loads.

$$\pi = U + V$$

where π denotes the total potential energy, U is the elastic strain energy, and V is the potential energy due to external loads. If P_1 and P_2 are forces acting on node 1 and 2, respectively, then

$$V = - P_1 u_1 - P_2 u_2$$

Substituting ε from Eq. (4.3), the total potential energy π becomes,

$$\pi = \frac{AE}{2} \left(\frac{u_2-u_1}{L}\right)^2 \int_0^L dx + \frac{AE}{2} \int_0^L \varepsilon_0^2 \, dx$$

$$- AE \left(\frac{u_2-u_1}{L}\right)^2 \int_0^L \varepsilon_0 \cdot dx + A \left(\frac{u_2-u_1}{L}\right) \int_0^L \sigma_0 dx$$

$$- P_1 u_1 - P_2 u_2 \qquad (4.4)$$

For a one-dimensional element ε_0 is the thermal strain given by,

$$\varepsilon_0(x) = \alpha\,[T(x) - T_i] \tag{4.5}$$

where α is the coefficient of thermal expansion, $T(x)$ is the element temperature distribution, and T_i is the initial temperature at the given prestress.

4.2.2 Potential Energy Minimization

To derive the element equation, the potential energy (Eq. (4.4)) is minimized with respect to the nodal displacements u_1 and u_2:

$$\frac{\partial \pi}{\partial u_1} = 0 \quad \text{and} \quad \frac{\partial \pi}{\partial u_2} = 0$$

or

$$\frac{AE}{L}(u_1 - u_2) = -\frac{AE}{L}\int_{\bullet}^{L} \varepsilon_0\,dx + A\,\sigma_0 + P_1$$

$$\frac{AE}{L}(-u_1 + u_2) = \frac{AE}{L}\int_{\bullet}^{L} \varepsilon_0\,dx - A\,\sigma_0 + P_2$$

The above two equations can be written in matrix form as,

$$\frac{AE}{L}\begin{bmatrix} 1 & -1 \\ -1 & 1 \end{bmatrix}\begin{Bmatrix} u_1 \\ u_2 \end{Bmatrix} = \frac{AE}{L}\begin{Bmatrix} -1 \\ 1 \end{Bmatrix}\int_{\bullet}^{L} \varepsilon_0\,dx + A\,\sigma_0\begin{Bmatrix} 1 \\ -1 \end{Bmatrix} + \begin{Bmatrix} P_1 \\ P_2 \end{Bmatrix} \tag{4.6}$$

For an isothermal element with constant temperature T, the thermal strain is,

$$\varepsilon_0 = \alpha\,(T-T_i) \tag{4.7}$$

and the above element equations reduce to,

$$\frac{AE}{L}\begin{bmatrix} 1 & -1 \\ -1 & 1 \end{bmatrix}\begin{Bmatrix} u_1 \\ u_2 \end{Bmatrix} = AE\alpha\,(T-T_i)\begin{Bmatrix} -1 \\ 1 \end{Bmatrix} + A\,\sigma_0\begin{Bmatrix} 1 \\ -1 \end{Bmatrix} + \begin{Bmatrix} P_1 \\ P_2 \end{Bmatrix} \tag{4.8}$$

4.3 Analysis Procedure

For a thermal-structural analysis of an orbiting space structure, the heating analysis and the thermal analysis are first performed to determine the temperature distribution in the structure. The prestress analysis is performed to compute element prestresses. Using the temperatures and prestresses, element Eqs. (4.8) are formulated and element matrix transformations from local to global coordinates are made. The element equations are then assembled to yield the system equations. Boundary conditions are imposed. Six boundary conditions are specified to constrain the structure from rigid body motion. The unknown nodal displacements are then solved, and element stresses are computed using Eqs. (4.1) and (4.3).

As the structure moves to another orbital position, the heating loads are recomputed, and the structural analysis is repeated. Such a sequence of computations is called a quasi-static analysis since dynamic

effects are neglected. A computational flowchart for the small deflection analysis is shown in Fig. 8.

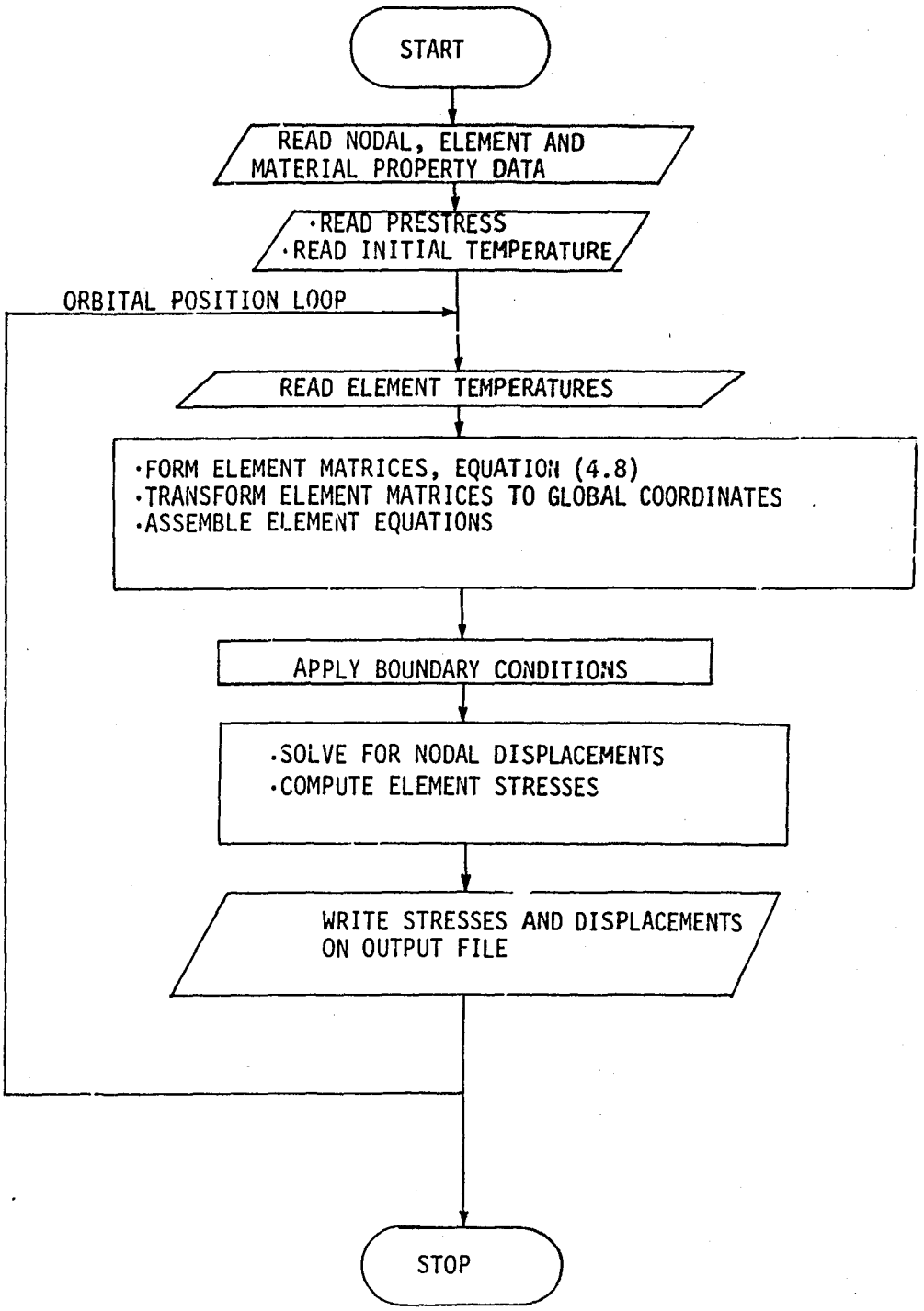

Fig. 8 Flowchart of small deflection structure analysis technique for orbiting structures.

Chapter 5

STRESS STIFFENING STRUCTURAL ANALYSIS

The small deflection (linear) structural analysis technique was described in Chapter 4 for cable-stiffened space structures. The assumption of small deflections was made in the strain-displacement relation. Since cables show nonlinear behavior as described in [15], the large deflection relation between strain and displacement must be used for the structural analysis of cable-stiffened large space structures. Using the large deflection relation between strain and displacements, the derivation of finite element equations in terms of displacements results in a nonlinear set of equations. The resulting stiffness matrix and right-hand side force vector contain displacements, prestress and thermal strain terms. Two solution algorithms for these nonlinear finite element equations are considered. The two techniques are stress stiffening described in this chapter and large deflection (nonlinear) technique described in Chapter 6. In the stress stiffening technique, only two iterations are performed whereas in the large deflection technique Newton-Raphson iteration is used until convergence is achieved.

Stress stiffening refers to changes in element stiffness due to element initial stress. This effect is also called geometric or initial stress stiffening. The change in element stiffness is due to the

presence of prestress and/or thermal strain terms in the stiffness matrix in contrast to the small deflection analysis where the stiffness matrix is an array of constants depending only on material properties and element geometry. The stress stiffening structural analysis is used because it normally provides a more accurate result than the linear analysis for cable-stiffened structures. A brief description of stress stiffening is given in [17]. In this chapter, a derivation of finite element equations for the stress stiffening analysis is first presented. A solution method for solving the unknown nodal displacements for an orbiting structure is then described.

5.1 Theory

The finite element equations for a stress stiffening structural analysis is derived using energy methods similar to the procedures for the linear analysis described in Chapter 4.

Figure 9 shows a rod or a cable element in global Cartesian XYZ coordinates. The strain-nodal displacements relation for large deflections is given by [18],

$$\varepsilon = \frac{u_2 - u_1}{L} + \frac{1}{2}\left(\frac{v_2 - v_1}{L}\right)^2 + \frac{1}{2}\left(\frac{w_2 - w_1}{L}\right)^2$$

or

$$\varepsilon = e + \frac{1}{2}\theta^2 + \frac{1}{2}\psi^2 \tag{5.1}$$

where u_1, v_1, w_1 and u_2, v_2, w_2 are nodal displacements in the elements local xyz directions at nodes 1 and 2, respectively, and e

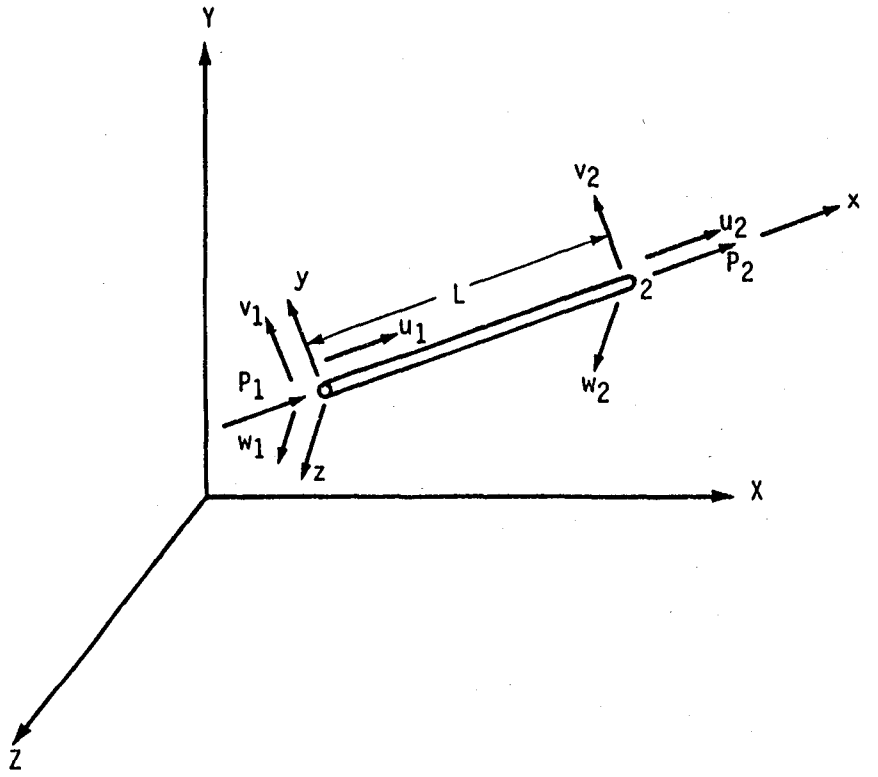

Fig. 9 One dimensional rod or cable element in local and global coordinates.

denotes axial strain; θ and ψ are rotations in the local x-y and x-z planes:

$$e = \frac{u_2 - u_1}{L} \tag{5.2a}$$

$$\theta = \frac{v_2 - v_1}{L} \tag{5.2b}$$

$$\psi = \frac{w_2 - w_1}{L} \tag{5.2c}$$

5.2 Element Equations

5.2.1 Element Potential Energy

The total potential energy is the sum of the elastic strain energy and the potential energy due to external forces. By substituting Eq. (5.1) into the elastic strain energy, Eq. (4.2), the total potential energy becomes,

$$\begin{aligned}\pi = {} & \frac{AEL}{2} e^2 + \frac{AEL}{2}\left[\left(e - \frac{1}{L}\int_0^L \varepsilon_0 dx + \frac{\sigma_0}{E}\right)\theta^2 + \frac{1}{4}\theta^4\right] \\ & + \frac{AEL}{2}\left[\left(e - \frac{1}{L}\int_0^L \varepsilon_0\, dx + \frac{\sigma_0}{E}\right)\psi^2 + \frac{1}{4}\psi^4\right] + \frac{AEL}{4}\theta^2\psi^2 \\ & - AEe\int_0^L \varepsilon_0\, dx + A\sigma_0 L e + \frac{AE}{2}\int_0^L \varepsilon_0^2\, dx \\ & - P_1 u_1 - P_2 u_2 \end{aligned} \tag{5.3}$$

5.2.2 Potential Energy Minimization

Element equations are derived by performing minimization of the total potential energy, Eq. (5.3), with respect to the nodal displacement components u_1, v_1, w_1, u_2, v_2, and w_2. As an example, minimization of the total potential energy with respect to u_1 is,

$$\frac{\partial \pi}{\partial u_1} = 0$$

or

$$\frac{AE}{L} u_1 + \frac{AE}{L}\frac{\theta}{2} v_1 + \frac{AE}{L}\frac{\psi}{2} w_1 - \frac{AE}{L} u_2 - \frac{AE}{L}\frac{\theta}{2} v_2$$

$$- \frac{AE}{L}\frac{\psi}{2} w_2 = - \frac{AE}{L} \int_L \varepsilon_0 \, dx + A \sigma_0 + P_1 \qquad (5.4)$$

For six nodal displacement components, the element equations are;

$$[K(u)] \{u\} = \{F\}_{\varepsilon_0} + \{F\}_{\sigma_0} + \{P\} \qquad (5.5)$$

where $[K(u)]$ is the stiffness matrix which depends on the unknown nodal displacements, $\{u\}$ is the unknown nodal displacement vector, $\{F\}_{\varepsilon_0}$, $\{F\}_{\sigma_0}$ and $\{P\}$ are the element force vectors due to thermal strain, prestress and the external applied forces, respectively. Details of these element matrices are shown in Appendix A.

5.3 Analysis Procedure

The finite element Eqs. (5.5) are nonlinear because the element stiffness matrix depends on the unknown nodal displacements. To solve these nonlinear equations an iterative technique is used. The stress stiffening method uses two iterations, [17]. For the first iteration, all nodal displacement components which appear in the element stiffness matrix are zero. Nodal displacement components computed in the first iteration are then used as the approximate solution for the second iteration which gives the stress stiffening result.

The stiffness matrix and load vectors are computed at each iteration. These element matrices are transformed from local to global coordinates, and the system equations are established. Appropriate boundary conditions are then imposed, and the unknown nodal displacements are computed. The first iteration nodal displacements are used as initial displacements to compute final displacements in the second iteration.

For the analysis of an orbiting space structure, the heating, thermal and prestress analysis are first performed. Displacements at the first orbital position are computed based on the given element temperatures, prestresses and initial temperatures. With these computed nodal displacements, the deformed structure is obtained and is used as the initial structural geometry to compute the structural deformation for the second orbital position. Prestresses and initial temperatures for each element are updated. At the second orbital position, the prestresses are the values of the final stresses of the first orbital position. Initial temperatures take the values of applied element

temperatures of the first orbital position. Similar computations are performed at each specified orbital position. A flowchart showing the stress stiffening structural analysis for an orbiting structure is given in Fig. 10.

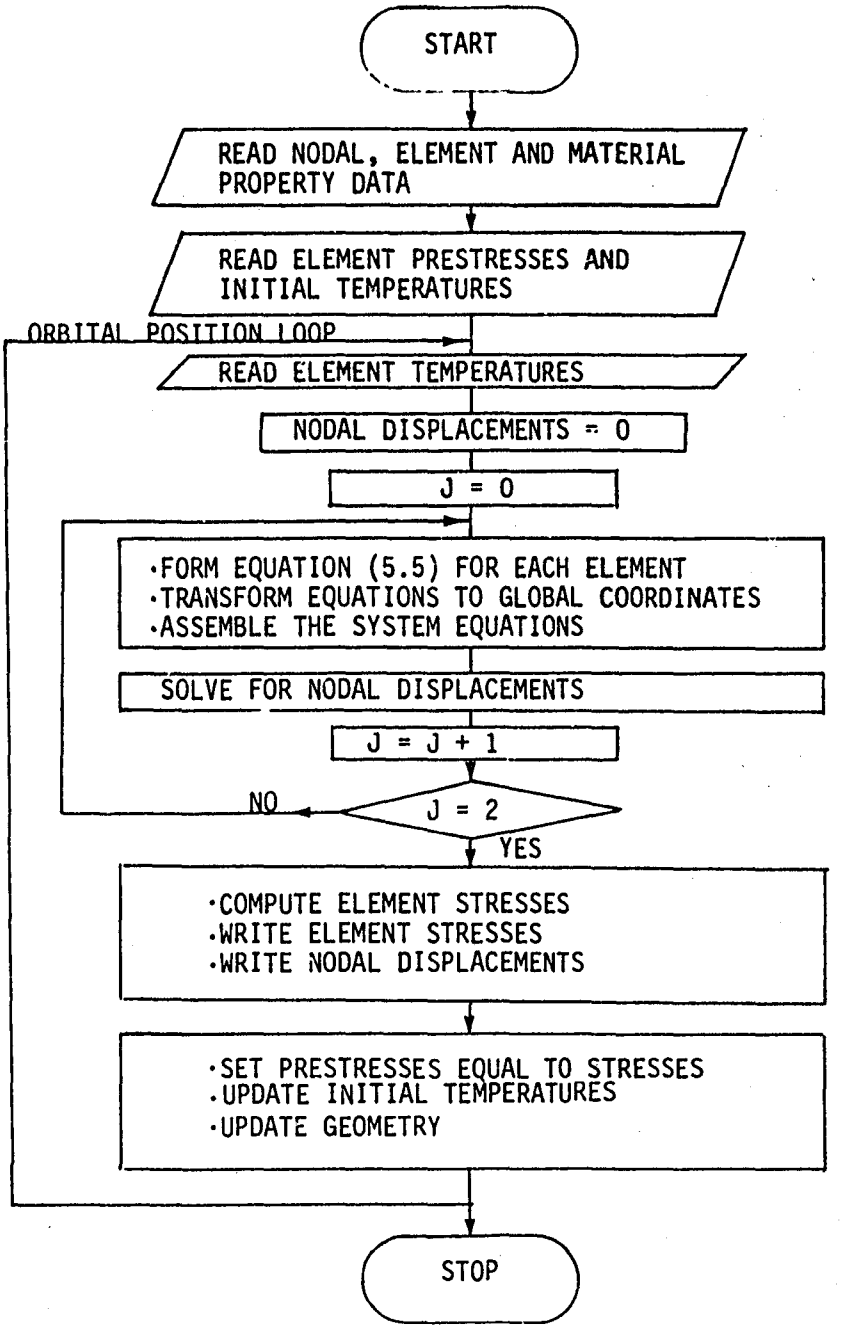

Fig. 10 Flowchart of the stress stiffening structural analysis for an orbiting space structure.

Chapter 6

LARGE DEFLECTION STRUCTURAL ANALYSIS

It was stated in Chapter 5 that the assumption of the large deflection relation between strain and displacement results in nonlinear finite element equations. One solution algorithm was described in Chapter 5. The second algorithm, the large deflection (nonlinear) technique is presented in this chapter. Large deflection structural analysis is normally used whenever the displacements are large enough such that the stiffness matrix based on the initial geometry does not represent the actual deformed structure. Reference [18] discusses theory and solution methods for large deflection analysis of structures due to simple loadings. Large deflection analysis provides high solution accuracy compared to the small deflection and the stress stiffening analysis for cable-stiffened structures, where each structural member is prestressed. Further explanation is presented in [17, 18]. The element equations obtained from large deflection analysis depend on nodal displacements leading to a nonlinear set of system equations. This chapter describes the solution method for the nonlinear equations. An analysis procedure for solving nodal displacements of the orbiting structure due to thermal loads is then explained.

6.1 Theory

The derivation of the finite element equation for large deflection structural analysis follows the procedures given in Chapter 5. The element equations are the same as Eqs. (5.5).

The element Eqs. (5.5) can be written in the form,

$$f_i(e, \theta, \psi) = 0, \qquad i = 1, 6 \tag{6.1}$$

where e is the axial strain; θ and ψ are the rotations in local x-y and x-z planes, respectively. In large deflection structural analysis, the Newton-Raphson iteration method is used to solve the above nonlinear equations. Application of the Newton-Raphson method to Eqs. (6.1) results in the following matrix equation, [19],

$$[J] \{\Delta u\} = \{R\} \tag{6.2}$$

where $[J]$ is the Jacobian matrix and $\{R\}$ is the residual load vector. The coefficients in the Jacobian matrix are given by,

$$J_{ij} = \frac{\partial f_i}{\partial u_i} \tag{6.3}$$

where u_j, $j = 1,6$ are the element nodal displacement components. The residual load vector is,

$$R_i = -f_i \tag{6.4}$$

6.2 Element Equations

To derive the element Eqs. (6.2), Eqs. (6.1) is first written. As an example, the first equation of Eqs. (6.1) is,

$$\frac{AE}{L} u_1 + \frac{AE}{L}\frac{\theta}{2} v_1 + \frac{AE}{L}\frac{\psi}{2} w_1 - \frac{AE}{L} u_2 - \frac{AE}{L}\frac{\theta}{2} v_2 - \frac{AE}{L}\frac{\psi}{2} w_2$$

$$+ \frac{AE}{L} \int_0^L \varepsilon_0 \, dx - A\sigma_0 - P_1 = 0$$

Using Eq. (6.3), the coefficients in the Jacobian matrix are,

$$J_{11} = \frac{\partial f_1}{\partial u_1} = \frac{AE}{L}$$

$$J_{12} = \frac{\partial f_1}{\partial v_1} = \frac{AE}{L} \cdot \frac{\theta}{2}$$

$$J_{13} = \frac{\partial f_1}{\partial w_1} = \frac{AE}{L} \cdot \frac{\psi}{2}$$

$$J_{14} = \frac{\partial f_1}{\partial u_2} = -\frac{AE}{L}$$

$$J_{15} = \frac{\partial f_1}{\partial v_2} = \frac{AE}{L} \cdot \frac{\theta}{2}$$

$$J_{16} = \frac{\partial f_1}{\partial w_2} = \frac{AE}{L} \cdot \frac{\psi}{2}$$

and the corresponding residual from Eq. (6.4) is,

$$R_1 = AEe + AE\left(\frac{\theta^2}{2} + \frac{\psi^2}{2}\right) + A\sigma_0 - \frac{AE}{L}\int^{L} \varepsilon_0 dx + P_1$$

Similarly, other coefficients in the Jacobian matrix and residual load vector can be derived, and the element equations can then be written in the form,

$$[J]^m \{\Delta u\}^{m+1} = \{\{R\}_{\varepsilon_0} + \{R\}_{\sigma_0} + \{R\}_e + \{R\}_{\theta,\psi} + \{R\}_p\}^m \qquad (6.5)$$

where $[J]^m$ is the Jacobian matrix, $\{\Delta u\}^{m+1}$ is the vector of nodal displacement increments, and the superscript m denotes the mth iteration. The right-hand side of the above equation contains residual load vectors associated with the thermal strain, element prestress, axial strain, rotational strain and external loads, respectively. The components of the Jacobian matrix and the residual load vectors are given in Appendix B. Once the nodal displacement increment is obtained, the new displacement vector is computed from,

$$\{u\}^{m+1} = \{u\}^{m} + \{\Delta u\}^{m+1} \tag{6.6}$$

Convergence criteria used is given as,

$$\frac{|\Delta u_i|}{|u_i|} < \text{tolerance} \tag{6.7}$$

where i denotes a typical displacement component. The convergence tolerance typically used herein is 10^{-2}.

6.3 Analysis Procedure

Element Jacobian matrices and residual load-vectors are computed at each iteration. Initial nodal displacements are set to zero at the first iteration. Element Jacobian matrices obtained in local coordinates are then transformed to global coordinates and then system equations are established. Appropriate boundary conditions are then imposed, and the unknown nodal displacement increments are computed. At each iteration the displacements are updated using Eqs. (6.6). The iteration process is terminated when convergence criteria given by Eqs. (6.7) are met.

For the analysis of an orbiting space structure, the heating, thermal, and prestress analyses are first performed. Displacements at the first orbital position are calculated based on the given element temperatures, prestresses and initial temperatures using the nonlinear analysis method discussed earlier. With these computed nodal displace-

ments, the deformed structure is obtained and is used as the initial structural geometry to compute the structural deformation for the second orbital position. Prestresses and initial temperatures are updated at each orbital position as discussed in Chapter 5. Nodal displacements and element stresses are computed similarly at each specified orbital position. A flowchart showing the large deflection structural analysis for an orbiting structure is shown in Fig. 11.

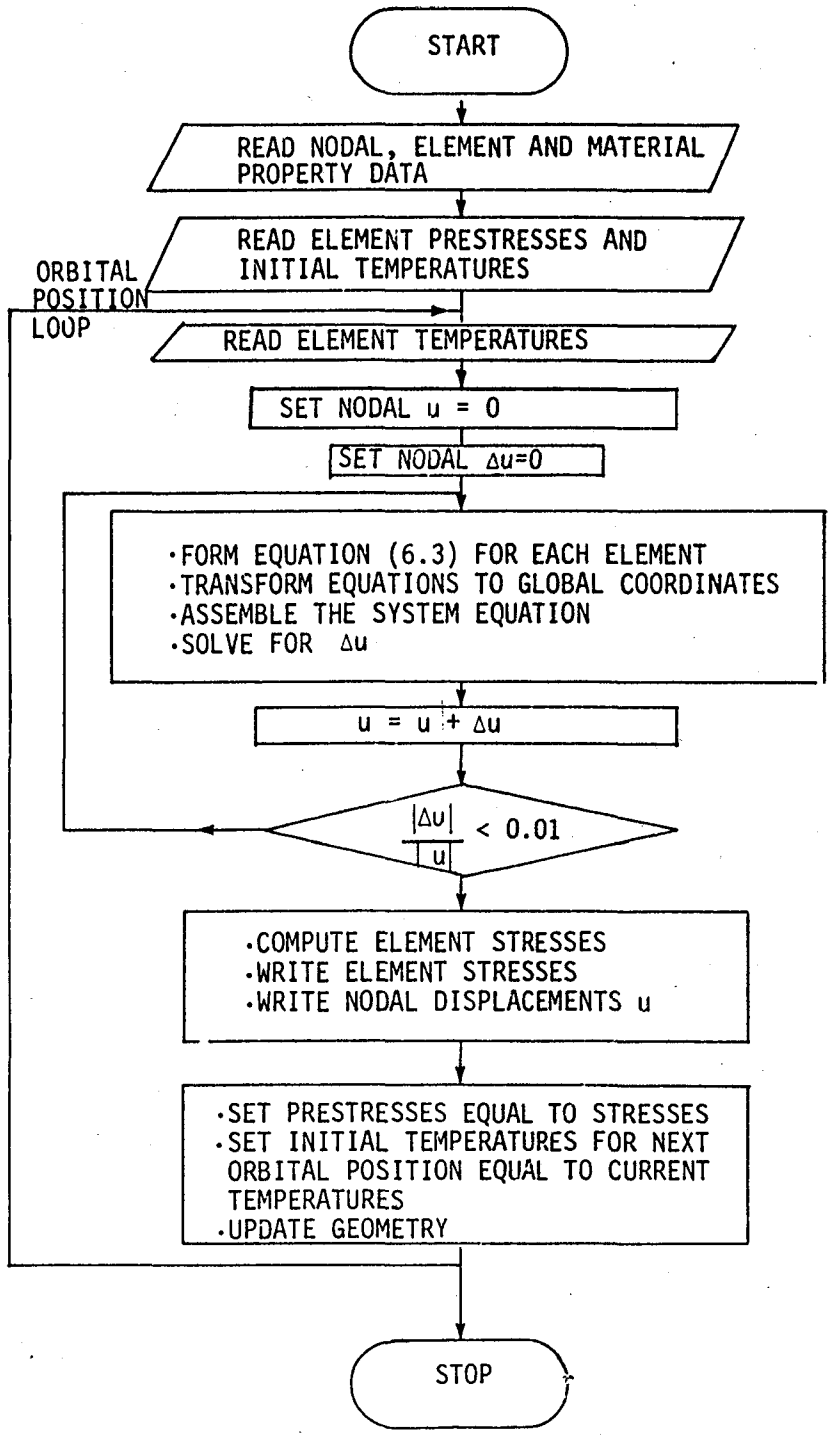

Fig. 11 Flowchart of large deflection structural analysis for an orbiting space structure.

Chapter 7

VERIFICATION OF STRUCTURAL ANALYSIS METHODS

In the preceding chapters, three structural analysis techniques were described. The accuracy of the small deflection, stress stiffening and large deflection analyses are verified in this chapter neglecting prestress effects. Two problems with known analytical solutions are used to verify the analyses. A nonlinear rod-spring system is analyzed first, and results from the three analysis techniques are compared with an analytical solution. A large displacement nonlinear analysis of an elastic cable is performed next, and results are compared with an analytical solution.

7.1 Nonlinear Rod-Spring System

Figure 12 shows the nonlinear rod spring system. Node 1 is hinged, node 3 is fixed, and node 2 can move only in the vertical direction. For an applied vertical force P, the vertical displacement u at node 2 can be computed from the exact relation [20],

$$P = ku + \frac{AE}{L}(L\sin\theta - u)\left[\frac{L}{(L\sin\theta)^2 + (L\sin\theta - u)^2} - 1\right] \qquad (7.1)$$

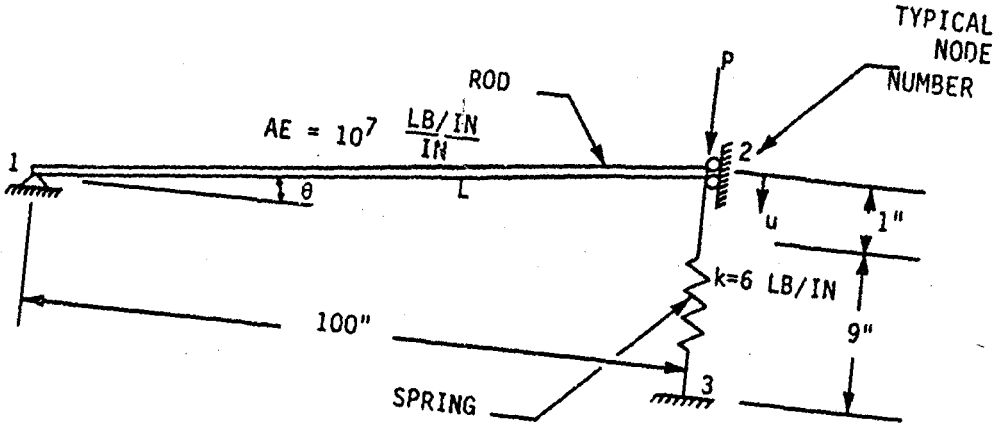

Fig. 12 Nonlinear rod-spring system.

where k is the spring constant, A, E and L are the cross-sectional area, the modulus of elasticity and the length of the rod, respectively; θ is the angle between the rod and the horizontal plane shown in Fig. 12.

Using the small deflection (linear), stress stiffening and large displacement (nonlinear) analyses, the displacement u is computed for different values of the applied force P. Results obtained using these analyses are compared with the analytical solution in Fig. 13.

For very small deflection (less than 0.25 inches), the displacement solution obtained from the linear, stress stiffening, and nonlinear analyses are close together. For larger deflections the three analyses show a wide difference in results. The nonlinear analysis provides very accurate displacement predictions for different loads, but the stress stiffening and linear analyses compare poorly with the analytical solution. The solution of the nonlinear rod-spring system verifies the nonlinear analysis technique and shows that linear analysis and stress stiffening analysis should not be used for such problems.

7.2 Symmetric Elastic Cable

A symmetrical elastic (aluminum) cable is shown in Fig. 14. The shape of the cable under its own weight neglecting the cable extension represents a catenary. Dimensions and material properties of the cable are given in Table 1. The cable is loaded by its own weight and is subjected to a rise in temperature of 200°F. The analytical solution

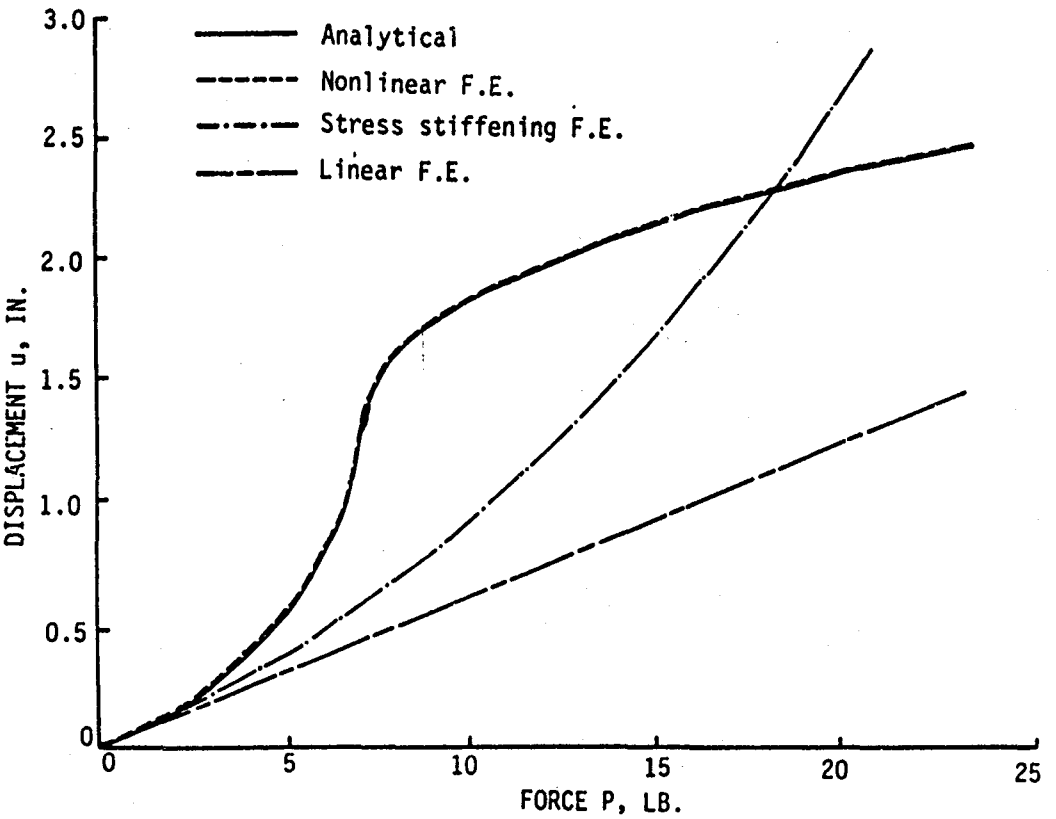

Fig. 13 Comparative displacement for nonlinear rod-spring system using three analysis techniques.

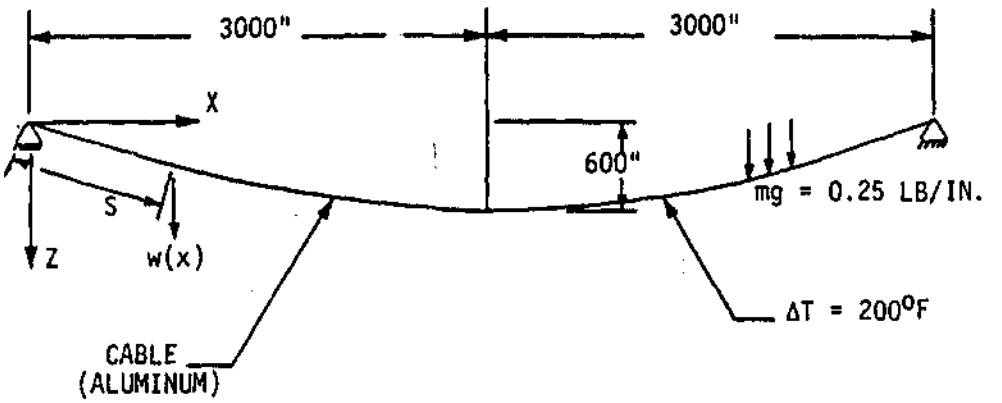

Fig. 14 A symmetric elastic cable.

Table 1

Dimensions and Material Properties of an Elastic Cable

GEOMETRY AND MATERIAL PROPERTY	VALUES
SPAN	6000 in.
SAG	600 in.
LENGTH	6157 in.
SPECIFIC WEIGHT	.11 lb/in.^{3}
WEIGHT/UNIT LENGTH	.25 lb/in.
CROSS-SECTIONAL AREA	2.5 in.^{2}
MODULUS OF ELASTICITY	10.0×10^6 psi
COEFFICIENT OF THERMAL EXPANSION	13.0×10^{-6}/F

for the displacement due to the cable's own weight and temperature increase is given in [15]. This analytical solution is obtained by first computing the undeformed shape of the inextensible cable by using,

$$Z(X) = \frac{H}{mg}\left[\cosh\left(\frac{mg\ell}{2H}\right) - \cosh\frac{mg}{H}\left(\frac{\ell}{2} - X\right)\right] \tag{7.2}$$

$$S(X) = \frac{H}{mg}\left[\sinh\left(\frac{mg\ell}{2H}\right) - \sinh\frac{mg}{H}\left(\frac{\ell}{2} - X\right)\right] \tag{7.3}$$

where H is the maximum horizontal component of force in the cable which is computed from,

$$\sinh\left(\frac{mg\ell}{2H}\right) = \frac{mgL_0}{2H} \tag{7.4}$$

where mg is the weight of the cable per unit length; X, Z and S are the horizontal distance, vertical distance and cable length, respectively, (Fig. 14). The length of the undeformed cable is L_0, and ℓ is the span.

The vertical deflection, including extension, due to the combined loading of the cable's weight and the temperature increase ΔT, with respect to the undeformed shape $Z(X)$, Eq. (7.2) is,

$$w = \left(\frac{mg\ell^2}{2H}\right)\left[\frac{\bar{h}}{(1-\bar{h})}\,\frac{X}{\ell}\left(1 - \frac{X}{\ell}\right)\right] \tag{7.5}$$

where $\bar{h}$ is the positive root of,

$$\bar{h}^3 - (2 + \theta + \frac{\lambda^2}{24})\,\bar{h}^2 + (1 + 2\theta + \frac{\lambda^2}{12})\,\bar{h} - \theta = 0 \qquad (7.6)$$

where

$$\theta = \alpha\,|\Delta T|\,L_t / (H\,L_e / E\,A)$$

$$\lambda^2 = (\frac{mg\ell}{H})^2 * \ell / (H\,L_e / E\,A)$$

$$L_t = \ell\,[1 + (\frac{mg\ell}{H})^2 / 12]$$

$$L_e = \ell\,[1 + 8\,(\frac{d}{\ell})^2]$$

α is the coefficient of thermal expansion, and d is the diameter of the cable.

The finite element solution of the cable problem is obtained using the nonlinear structural analysis technique. The geometric symmetry of the problem is used where only half of the cable is modeled for the analysis. The finite element model includes 25 cable elements and 26 nodes. The nonlinear technique using Newton-Raphson iteration method (Chap. 6), converges in five interations.

The vertical deflections for the analytical and finite element solution are compared in Fig. 15. The nonlinear finite element solution provides very accurate results with a maximum difference of 0.05 percent.

The results of these two problems verify that the large deflection

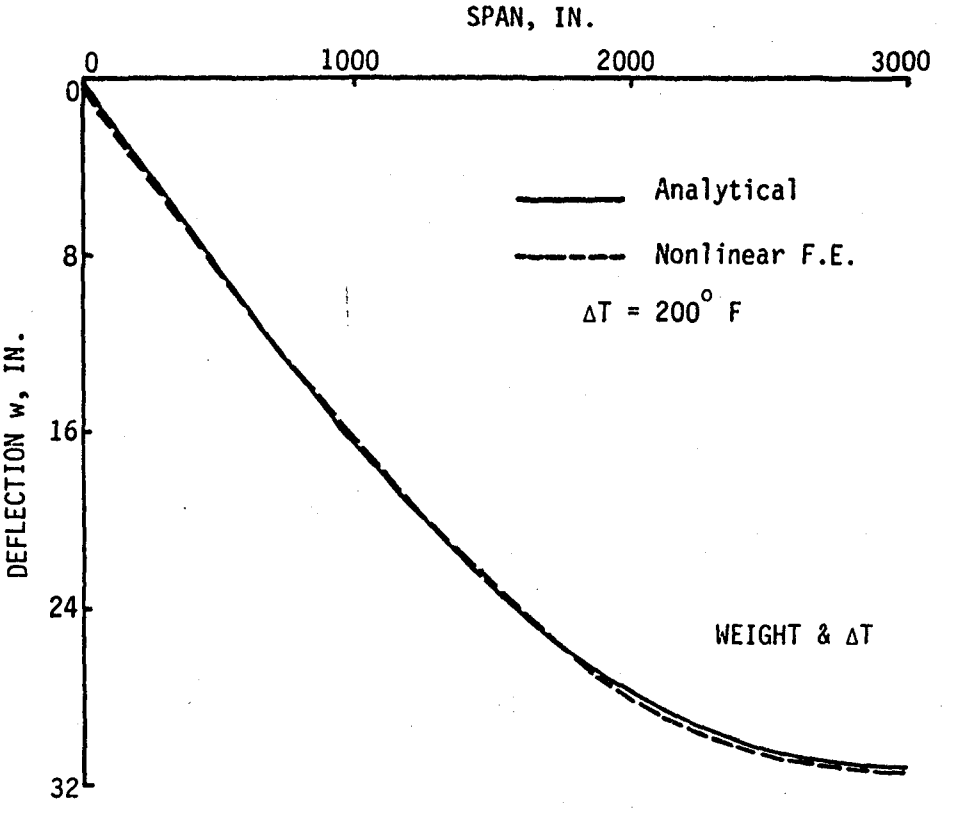

Fig. 15 Comparative deflections for cable loaded by its own weight and subjected to a temperature rise.

(nonlinear) finite element analysis can be used to analyze cable deflection accurately. The linear and stress stiffening analyses techniques may not provide results of comparable accuracy for such nonlinear problems.

The two problems analyzed did not consider prestress effects that characterize cable applications in large space structures. In the next chapter, cable-stiffened orbiting structures will be analyzed. The three analysis methods will be evaluated for these applications including prestress effects.

Chapter 8

THERMAL-STRUCTURAL ANALYSIS OF CABLE-STIFFENED ORBITING SPACE STRUCTURES

This chapter is devoted to the analysis of cable-stiffened orbiting space structures. Small deflection (linear), stress stiffening and large deflection (nonlinear) analyses procedures were described in Chapters 4, 5, and 6, respectively. Chapter 7 demonstrates for two structures without prestress, that the nonlinear analysis provides more accurate displacements than the stress stiffening and the linear analysis procedures. It was also verified that the nonlinear analysis provides very accurate displacements for a thermal load.

Thermal-structural analysis of prestressed cable-stiffened space structures is described in this chapter. Comparative analyses for two typical cable-stiffened structures are presented. The analyses were performed using linear, stress stiffening and nonlinear techniques, and the results are compared in tables and figures. The analyses are performed at different structural prestress levels to study the effect of prestress.

8.1 Simplified Two-Dimensional Pretensioned Cable System

A simplified two-dimensional pretensioned cable system is shown in Fig. 16. The cables which form the parabolic shape are called radial

NODE	1	2	3	4	5
X	3.37	10.1	23.8	38.0	52.7
Y	-9.6	-9.4	-8.9	-6.8	-3.7

(DIMENSIONS ARE IN METERS)

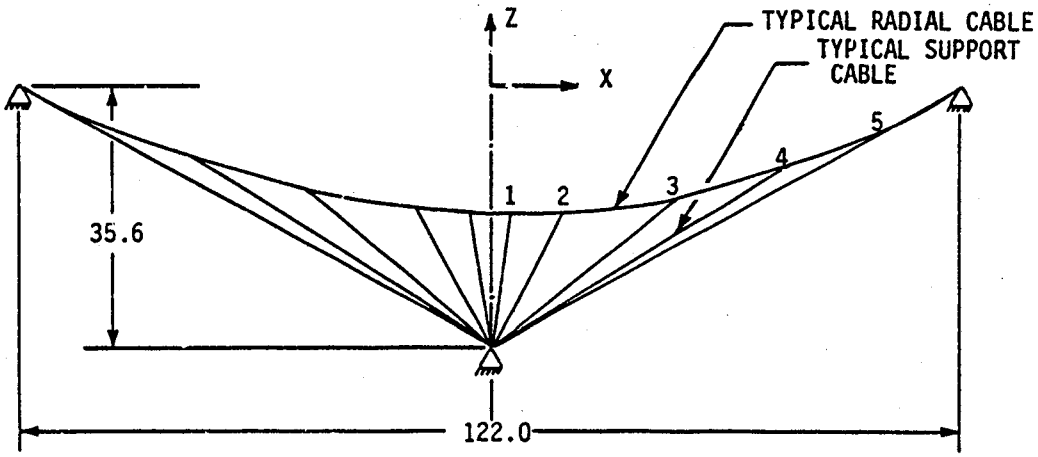

Fig. 16 Simplified two-dimensional pretensioned cable system.

cables, and the cables which support these are called the support cables. All cables are made of graphite epoxy, where the material properties are given in Table 2. The finite element model of the structure consists of 21 elements and 13 nodes.

8.1.1 Heating and Thermal Analysis

The cable system is assumed to be in a geosynchroncus earth-facing orbit as shown in Fig. 17. Heating histories for two typical structural members are shown in Fig. 18. The member incident heating is maximum when the member is perpendicular to the solar vector. The member heating drops when the member is either parallel to the solar vector or in the earth's shadow. The heating rate varies from 1200 W/m^2 to 10 W/m^2 for a typical member during the orbit.

Member heat loads are used to compute member temperatures in the thermal analysis. Isothermal elements are used because members are made of graphite epoxy which have very low thermal conductivity. Figure 19 shows temperature histories of two typical members. The temperature histories follow the patterns of the member heating histories because the members change orientation slowly with respect to the solar flux. The member's low mass and high surface emissivity along with the slow change in heating produce member temperatures very close to the radiation equilibrium temperatures throughout the orbit. When the structure enters the earth's shadow, member temperatures drop suddenly and approach much lower radiation equilibrium temperatures. When the structure leaves the earth's shadow, member temperatures rise abruptly due to

Table 2

Properties of Simplified Two-Dimensional Pretensioned Cable System

Radial cable diameter	3.09 mm
Support cable diameter	1.21 mm
Modulus of elasticity	1.23×10^{11} N/m^2
Coefficient of thermal expansion	5.40×10^{-7} 1/K
Density	1650.0 kg/m^3
Specific heat	879.2 J/kg-K
Emmissivity	0.84
Absorbtivity	0.916

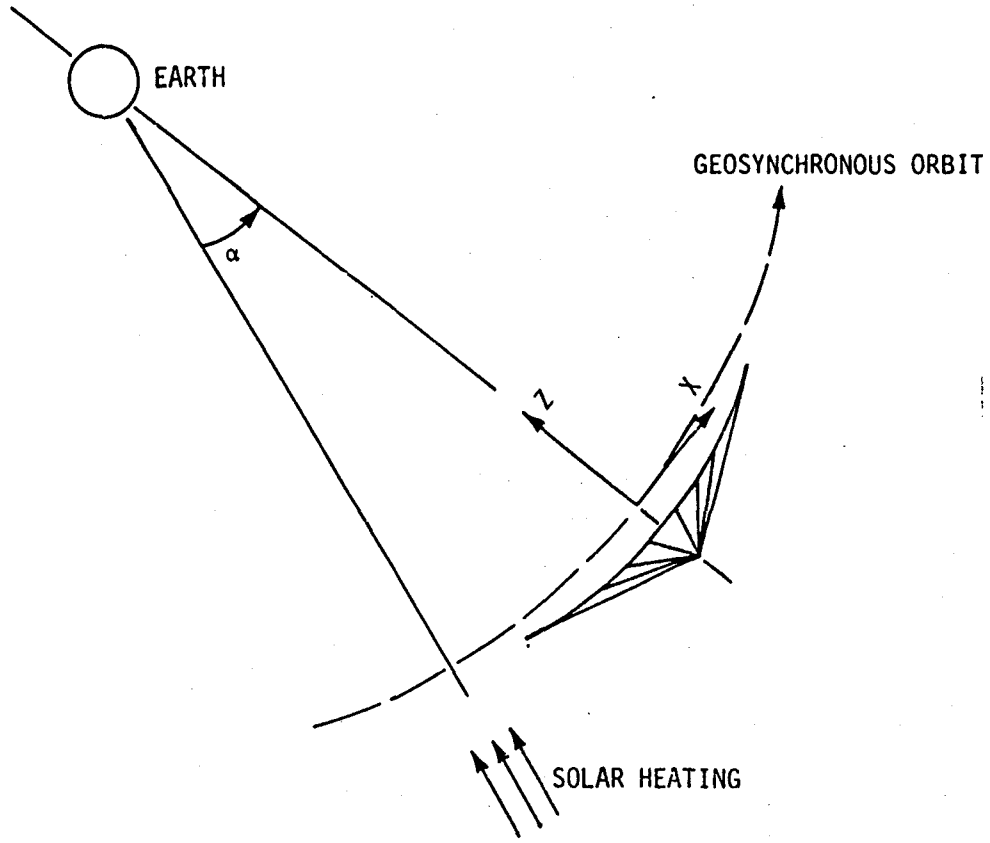

Fig. 17 Orientation of simplified pretensioned cable system in geosynchronous orbit.

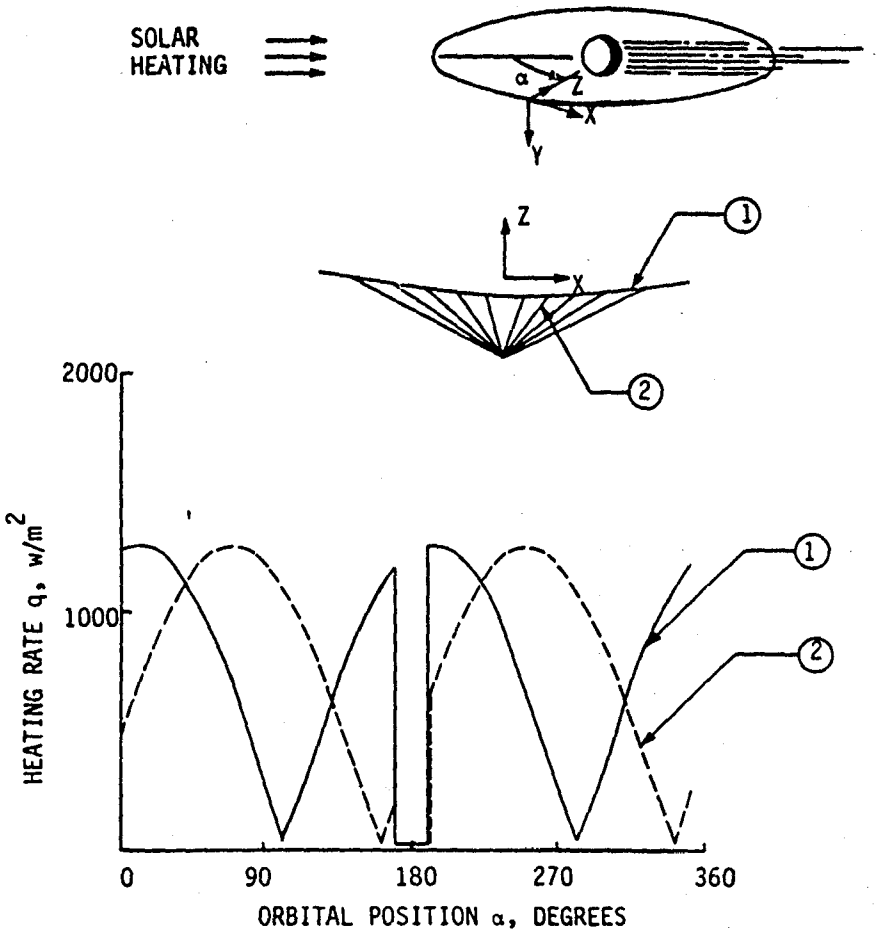

Fig. 18 Heating histories of typical members of simplified pretensioned cable system.

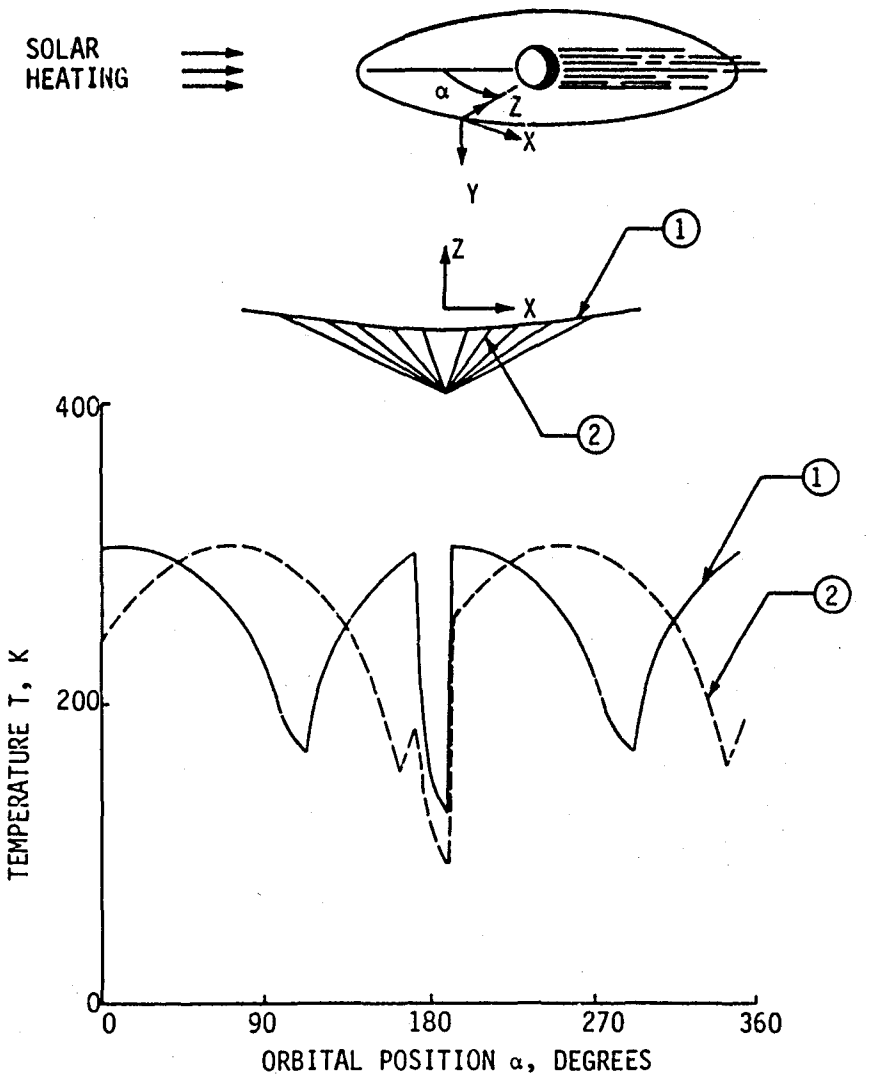

Fig. 19 Temperature histories of typical members of simplified pretensioned cable system.

the abrupt change of heat load. The range of member temperatures during an entire orbit is from 320 K to 90 K. The member temperatures at the different orbital positions are used in the structural analysis to compute displacements and stresses.

8.1.2 Prestress Analysis

Element prestresses are computed using the prestress analysis procedure described in Chapter 3. Geometric symmetry of the structure is used, and a tensile force of 452 N is specified for element number one (see Fig. 20). The prestress program is then used to compute the other element forces and stresses. Figure 20 shows the computed forces and prestresses for each member of the symmetric structure.

8.1.3 Structural Analysis

Linear, stress stiffening and nonlinear analyses are used for computation of structural deformations and cable stresses. Element temperatures and element prestresses calculated earlier are used as input data in these analyses. Initial member temperatures of 294 K are assumed. Analyses are performed at orbital positions for the orbit as described in the analysis procedures in Chapters 4, 5, and 6. The three analyses predict similar patterns of nodal displacements and member stresses. Only the results of the nonlinear analysis is presented in the figures. Deflection comparisons for the three analyses are presented in tabular form in the next section.

Figure 21 shows the displacement histories of two typical nodes. The nodal displacement history for a typical node follows the temper-

ELEMENT NO.	FORCE (N)	PRESTRESS (MPa)
1	452.0	60.2
2	173.3	23.1
3	150.2	20.0
4	134.6	17.9
5	134.1	17.8
6	133.6	17.8
7	284.5	245.4
8	25.8	22.2
9	21.5	18.5
10	1.0	0.9
11	4.0	3.4

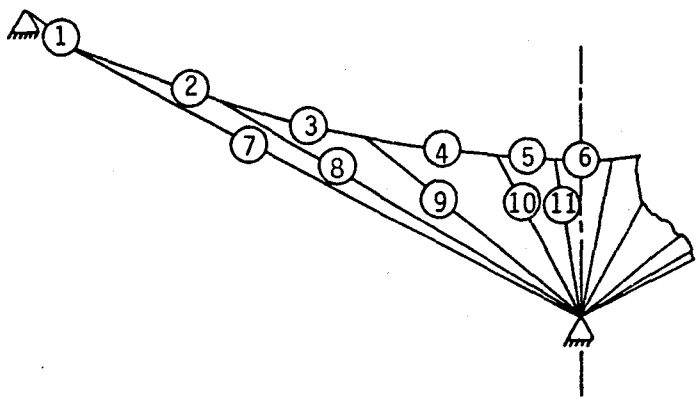

Fig. 20 Member prestresses for symmetric simplified pretensioned cable system.

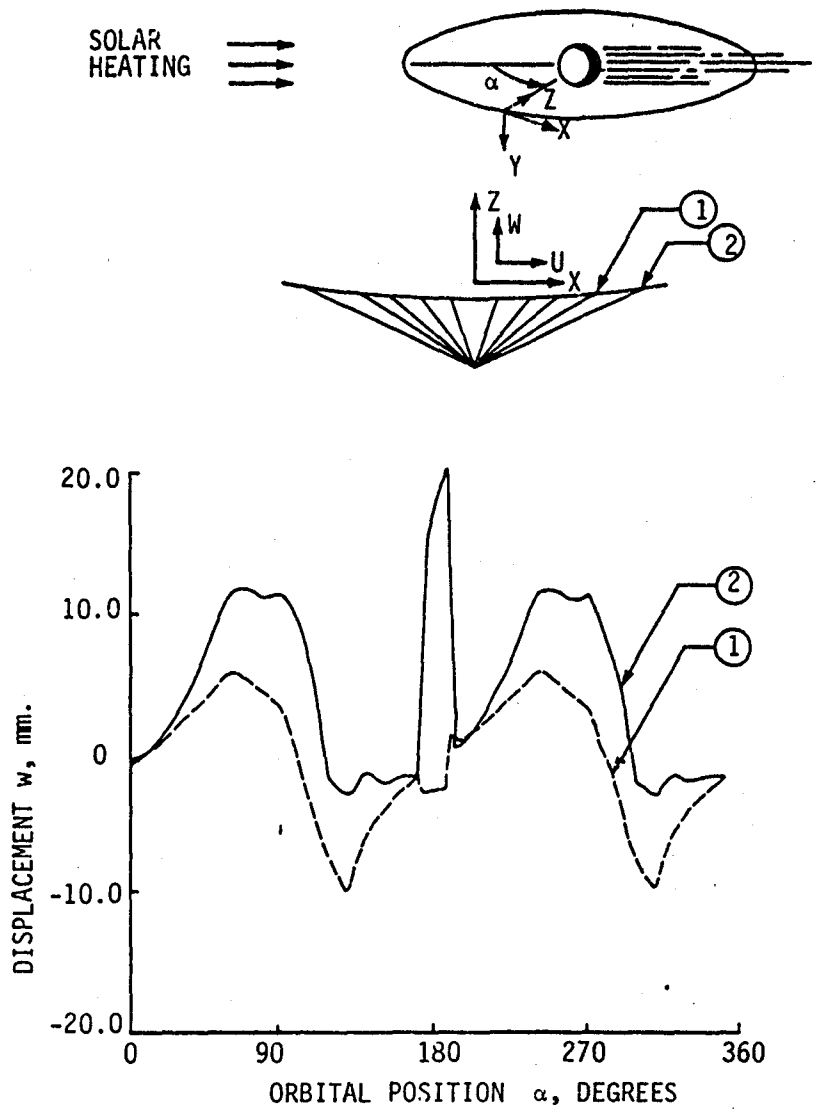

Fig. 21 Displacement histories for two typical nodes on simplified pretensioned cable system.

ature histories of the connected elements (not shown). Figure 22 shows the stress histories for two typical members. The stress variation during the orbit is small compared to the prestress level of the member. For a typical member, the stress variation is 11 percent from its prestress value. The maximum stress change occurs during passage through the earth's shadow.

Greatly exaggerated deformed shapes of the structure at the 0, 90, and 130 degrees orbital positions are shown in Fig. 23. The deformed shape of the structure is in equilibrium and members are in tension. The deflection of the parabolic surface is not symmetric because the symmetrical elements have unequal thermal loads at different orbital positions. Maximum displacements are in the Z direction. At the 90 degrees orbital position, a maximum displacement of 11.5 mm (shown in Fig. 23) occurs at the node nearest to the support. A maximum Z-displacement of 20 mm occurs at the same node during passage through the earth shadow.

8.1.4 Comparative Deformations

To compare the three structural analysis methods, the thermal-structural analysis is performed at three prestress levels using the linear, stress stiffening and nonlinear analysis techniques. The first prestress level is determined by specifying a force of 45.2 N for member number one (see Fig. 20). Similarly, the second and the third prestress levels are determined by specifying forces of 452 N and 4520 N, respectively. The second prestress level is close to the design prestress

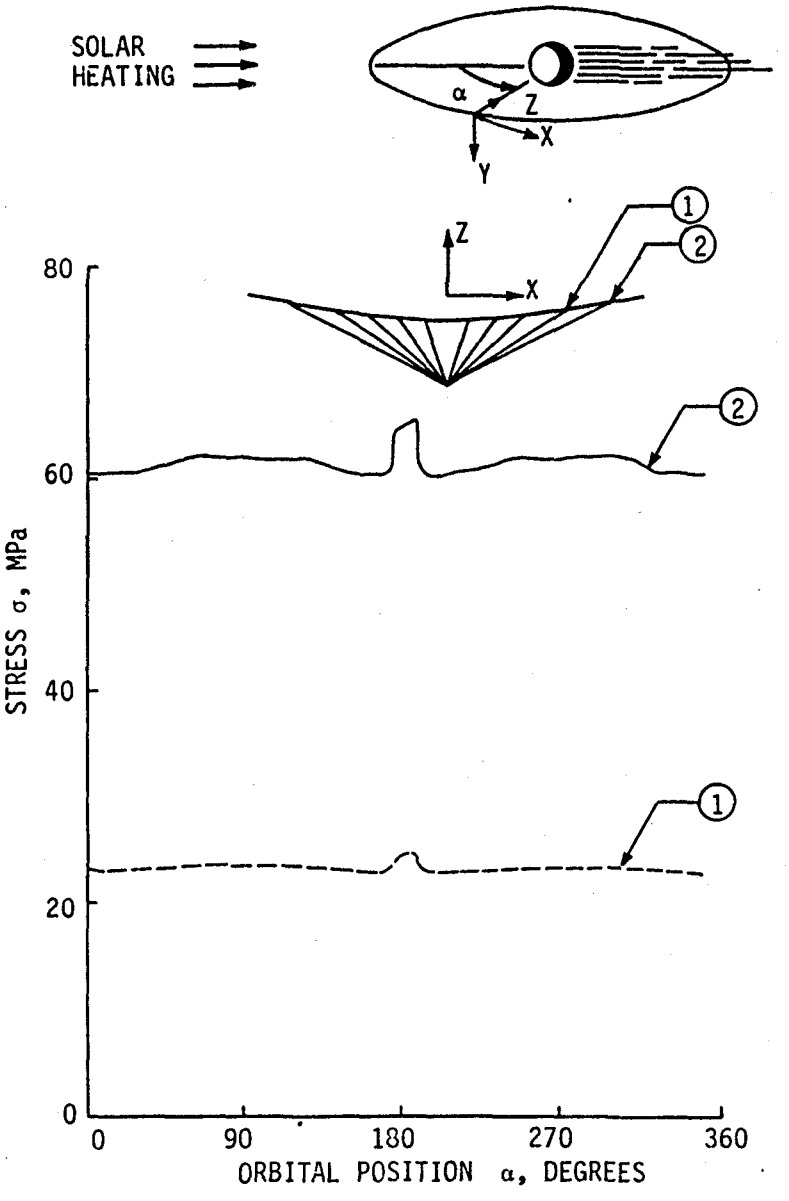

Fig. 22 Stress histories for two typical members of the simplified pretensioned cable system.

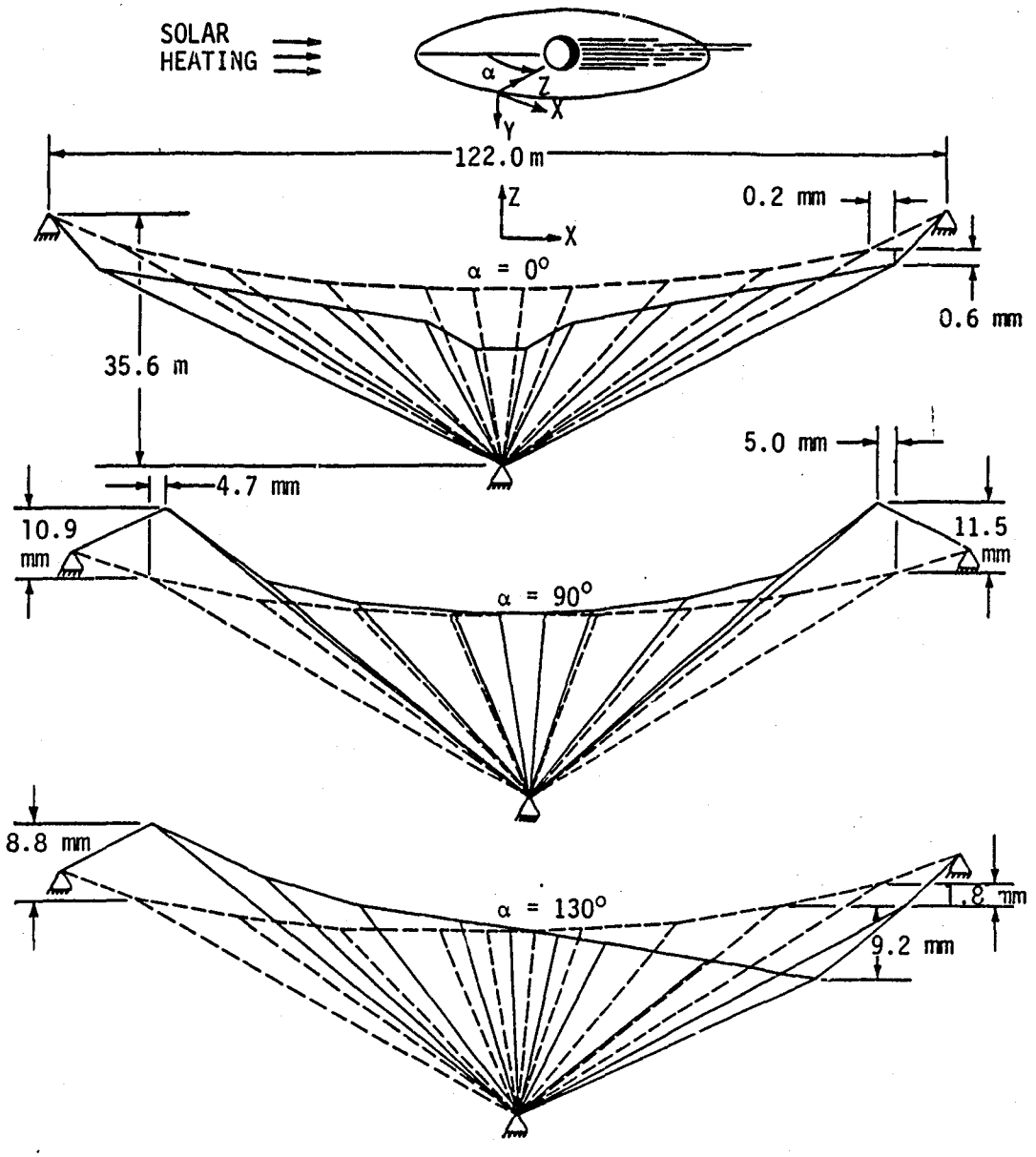

Fig. 23 Deformation of the simplified pretensioned cable system at different orbital positions.

used by NASA for structures such as the hoop column antenna [1]. The third prestress level is a hypothetical prestress level assumed for evaluation of the three structural analysis techniques. At this prestress some of the members may exceed design allowable stresses in tension.

Comparative deflections for node five (see Fig. 16) obtained from the three analysis techniques at the orbital positions of 0, 90, and 187 degrees are shown in Table 3. For these prestress levels, the linear analysis overestimates the deflection compared to the stress stiffening and nonlinear analysis. With increasing prestress, the linear analysis results remain almost unchanged, but the stress stiffening and nonlinear analysis results vary significantly. The latter two analyses predict relatively small deflections at higher prestress.

For the second prestress level at the 90 degrees orbital position, the linear and stress stiffening analyses predict 15 percent and 0.31 percent higher displacements than the nonlinear analysis, respectively. As prestress increases, the error in the linear analysis increase and results are not acceptable. The errors in the stress stiffening analysis increase also but remain within acceptable levels. The stress stiffening analysis can be used at NASA design values of prestresses with small error.

8.2 Three-Dimensional Prestressed Hoop Column Antenna

A three-dimensional hoop column antenna is shown in Fig. 24. Dimensions of the finite element model are shown on the front and top

Table 3

Simplified Pretensioned Cable System
(Fig. 16) Z-Deflection Comparison (mm)

ORBITAL POSITION (DEGREES)	0	90	187
PRESTRESS LEVEL ONE (F_1^* = 45.2 N)			
LINEAR ANALYSIS	-.6590	13.40	22.97
STRESS STIFFENING ANALYSIS	-.6592	12.90	22.80
NONLINEAR ANALYSIS	-.6536	13.10	22.80
PRESTRESS LEVEL TWO (F_1 = 452.0 N)			
LINEAR ANALYSIS	-.6578	13.40	22.97
STRESS STIFFENING ANALYSIS	-.6332	11.69	20.98
NONLINEAR ANALYSIS	-.6097	11.66	20.95
PRESTRESS LEVEL THREE (F_1 = 4520.0 N)			
LINEAR ANALYSIS	-.6461	13.41	22.98
STRESS STIFFENING ANALYSIS	-.4769	6.738	11.87
NONLINEAR ANALYSIS	-.3831	6.668	11.78

*F_1 is pretension in member one (see Fig. 20).

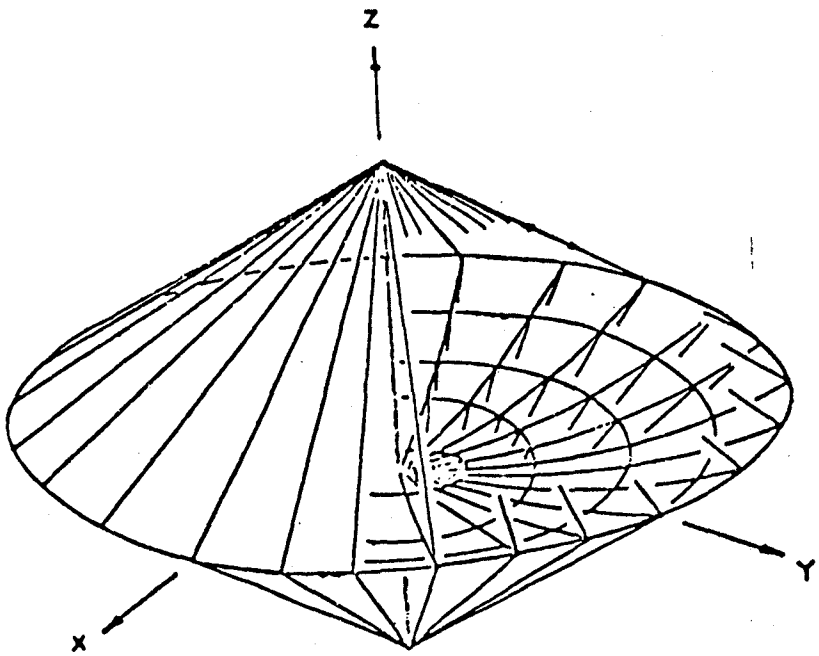

Fig. 24 Three-dimensional prestressed hoop column antenna.

views in Figs. 25 and 26. Tables 4 and 5 provide member cross-sectional areas and material properties. The finite element model consists of 123 nodes and 387 elements. The hoop and column are represented by rod elements, and cables are represented by cable elements. In addition, 192 fictitious cable elements were added for structure stability. The fictitious cable elements have very low (10^6 N/m^2) modulus of elasticity compared to the other elements of the structure (10^{11} N/m^2) and have zero coefficient of thermal expansion.

The structure is in a geosynchronous orbit oriented as shown in Fig. 27 with the antenna surface pointing towards the earth. The analysis of the three-dimensional prestressed hoop column antenna is performed similar to the simplified two-dimensional pretensioned cable system described in the previous section. The heating analysis and thermal analysis are performed at different orbital positions up to orbital angle of 200 degrees. A temperature variation from 310 K to 90 K is observed for a typical member during passage through the earth shadow.

8.2.1 Prestress Analysis

The structure's geometric symmetry is used in the prestress analysis. Symmetrical elements and nodes are identified and grouped in element and nodal groups. Six member forces are specified for the structure, and the prestress program is used to compute other member forces and stresses. These computed stresses are used as the member prestresses in the structural analysis. The fictitious elements have no prestresses. Figure 28 shows member prestresses and forces in a typical section of the structure.

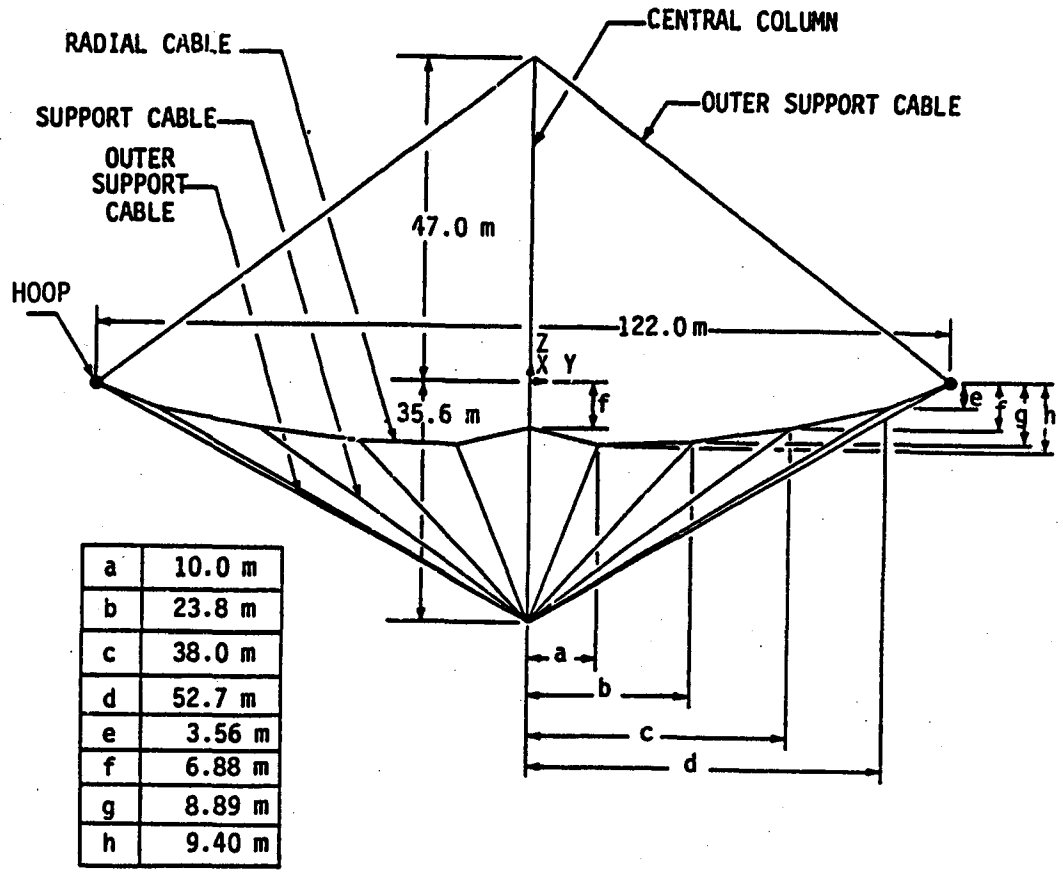

a	10.0 m
b	23.8 m
c	38.0 m
d	52.7 m
e	3.56 m
f	6.88 m
g	8.89 m
h	9.40 m

Fig. 25 Front section of the hoop column antenna.

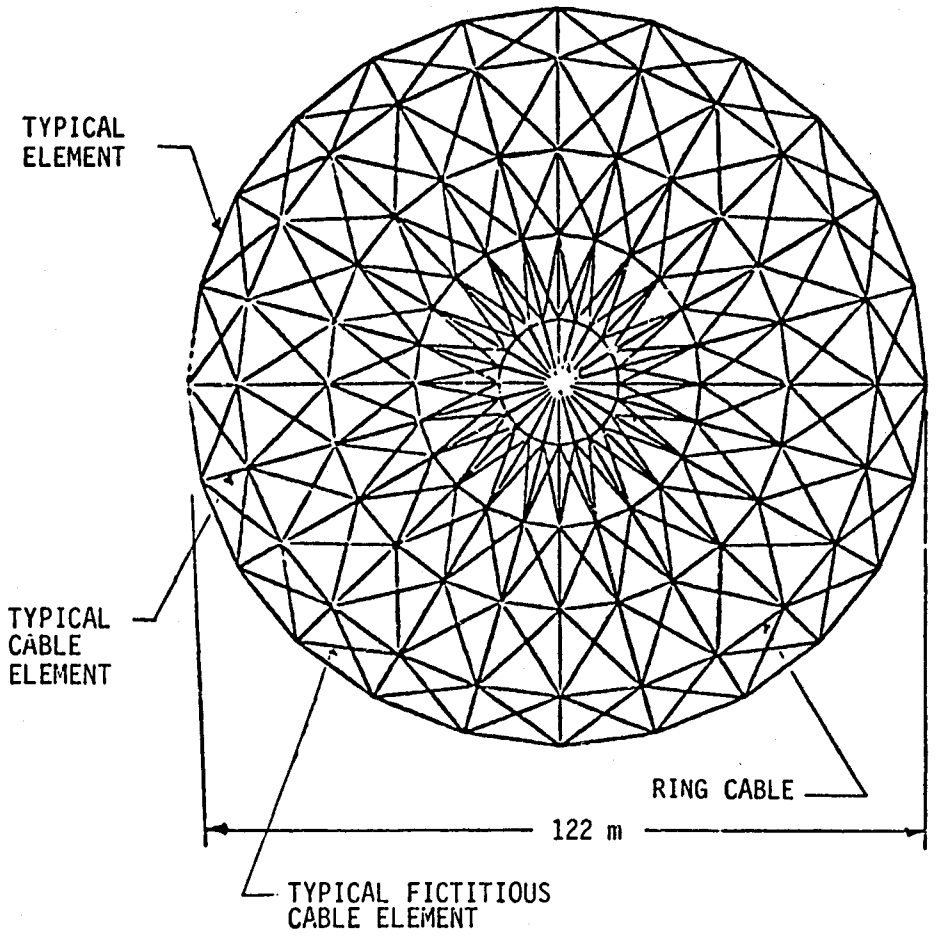

Fig. 26 Top view of the finite element model of the prestressed hoop column antenna.

Table 4

Hoop Column Antenna Cross-Sectional Areas and Materials

STRUCTURAL MEMBER	AREA (m^2) x 10^{-6}	MATERIAL
CENTRAL COLUMN (HOLLOW TUBE)	237.6	GRAPHITE EPOXY-1
HOOP (HOLLOW TUBE)	266.0	GRAPHITE EPOXY-2
OUTER SUPPORT CABLE, COLUMN TO HOOP (+ Z SIDE)	27.3	QUARTZ
OUTER SUPPORT CABLE, COLUMN TO HOOP (- Z SIDE)	4.63	GRAPHITE EPOXY-1
RADIAL CABLE, RING TO RING	7.49	GRAPHITE EPOXY-1
SUPPORT CABLE COLUMN TO RING	1.15	GRAPHITE EPOXY-1
RING CABLE	0.297	GRAPHITE EPOXY-1

Table 5

Material Properties of Hoop Column Antenna

	GRAPHITE EPOXY-1	GRAPHITE EPOXY-2	QUARTZ
Modulus of elasticity $x10^{10}$ N/m^2	12.30	7.30	5.25
Coefficient of thermal expansion $x\ 10^{-7}/K$	-7.2	7.2	5.4
Density $x10^3$ kg/m^3	1.60	1.93	1.74
Specific heat Joule/kg-K	879.2	879.2	840.0
Emissivity	0.84	0.84	0.93
Absorbtivity	0.916	0.916	0.916

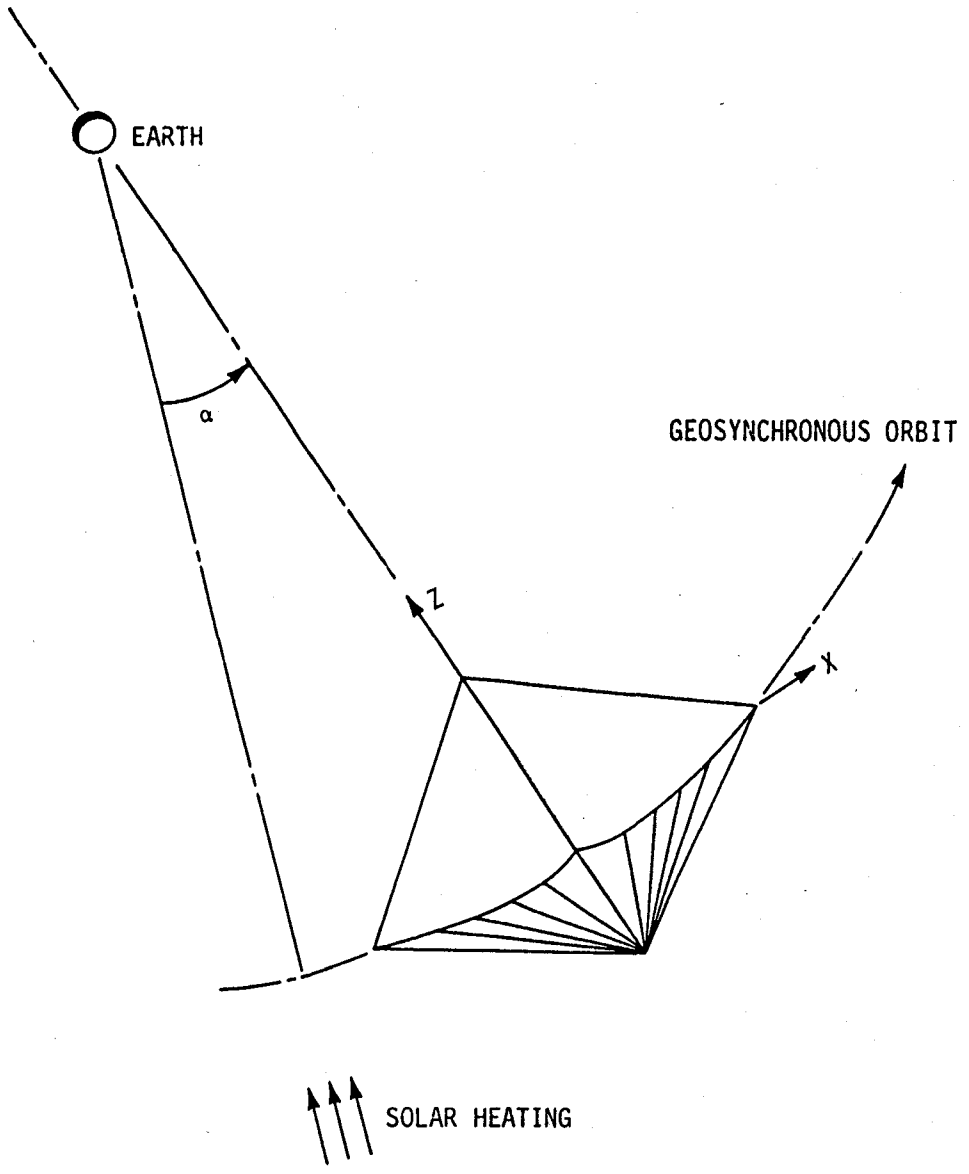

Fig. 27 Orientation of prestressed hoop column antenna in earth orbit.

ELEMENT NO.	FORCE (N)	PRESTRESS (MPa)
1	121.7	16.2
2	134.1	17.8
3	154.2	20.5
4	189.1	25.2
5	452.0	60.2
6	37.1	32.0
7	22.2	19.1
8	33.2	28.6
9	26.2	226.5
10	140.0	30.2
11	407.5	14.8
12	-5968.4	-25.1
13	-6681.1	-28.1
14	-3291.3	-12.3
15	25.0	84.0
16	20.0	67.2
17	15.0	50.4
18	10.0	33.6

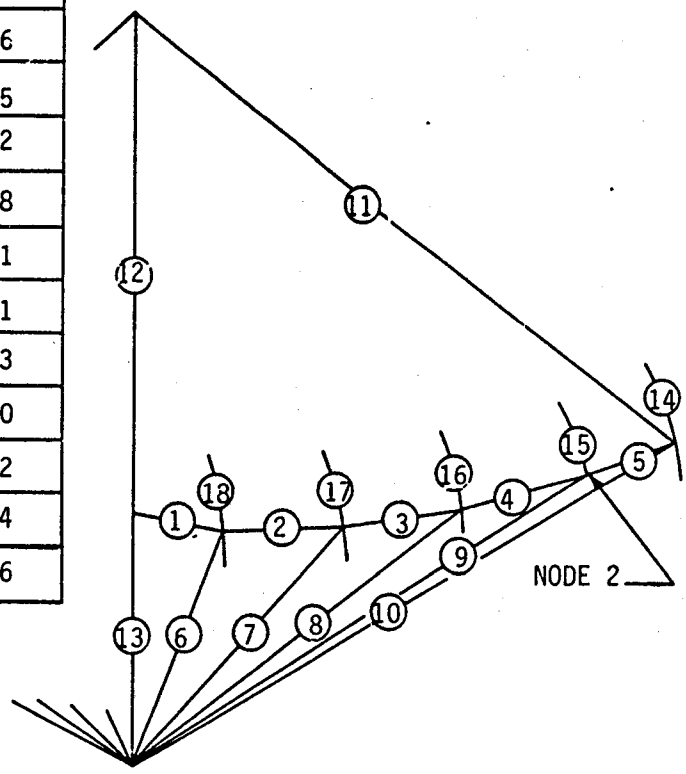

Fig. 28 Member prestresses for prestressed hoop column antenna.

8.2.2 Structural Analysis

Using temperatures and prestresses, the linear, stress stiffening and nonlinear analyses are performed to compute nodal deflections and member stresses at different orbital positions. The three analyses predict similar patterns of nodal displacements and member stresses. The results of the nonlinear analysis is presented in the figures. Deflection comparisons for the analysis are presented in tabular form in the next section. The hoop and antenna of the structure are in compression at all times during the orbit. Buckling of these members has not been considered.

Figure 29 shows the Z-displacement histories for two typical nodes on the antenna's surface. During orbit, points on the antenna's surface move toward and away from the earth, i.e. ± Z displacements take place. A maximum Z deflection of 20 mm occurs at a node on the antenna's surface nearest to the hoop in the earth's shadow. A significant displacement of 15 mm occurs at the same node at 90 degrees orbital position. The Z-deflections of the antenna surface at three orbital positions are shown in Fig. 30. Figure 31 shows the Z deflections of 4 panels at the 90 degree orbital position. Figure 32 shows displacement contours on the antenna's surface. The figures show that antenna surfaces near the hoop have maximum deflection. The displacements are not exactly axisymmetric as they vary from panel A to D (Fig. 31). Displacements in the central region of the antenna's surface are small. Stress variation for a typical element is ±8 percent from a prestress value of 60 MPa.

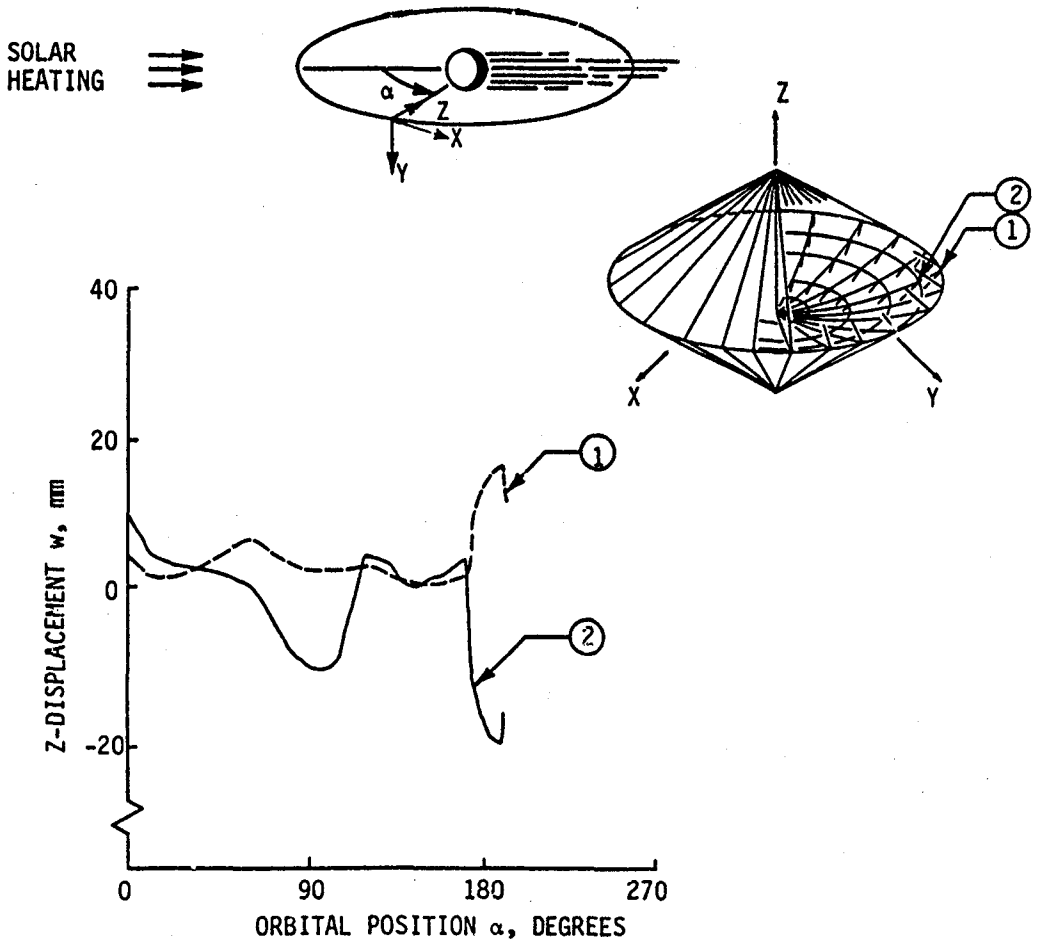

Fig. 29 Displacement histories for two typical nodes on the prestressed hoop column antenna.

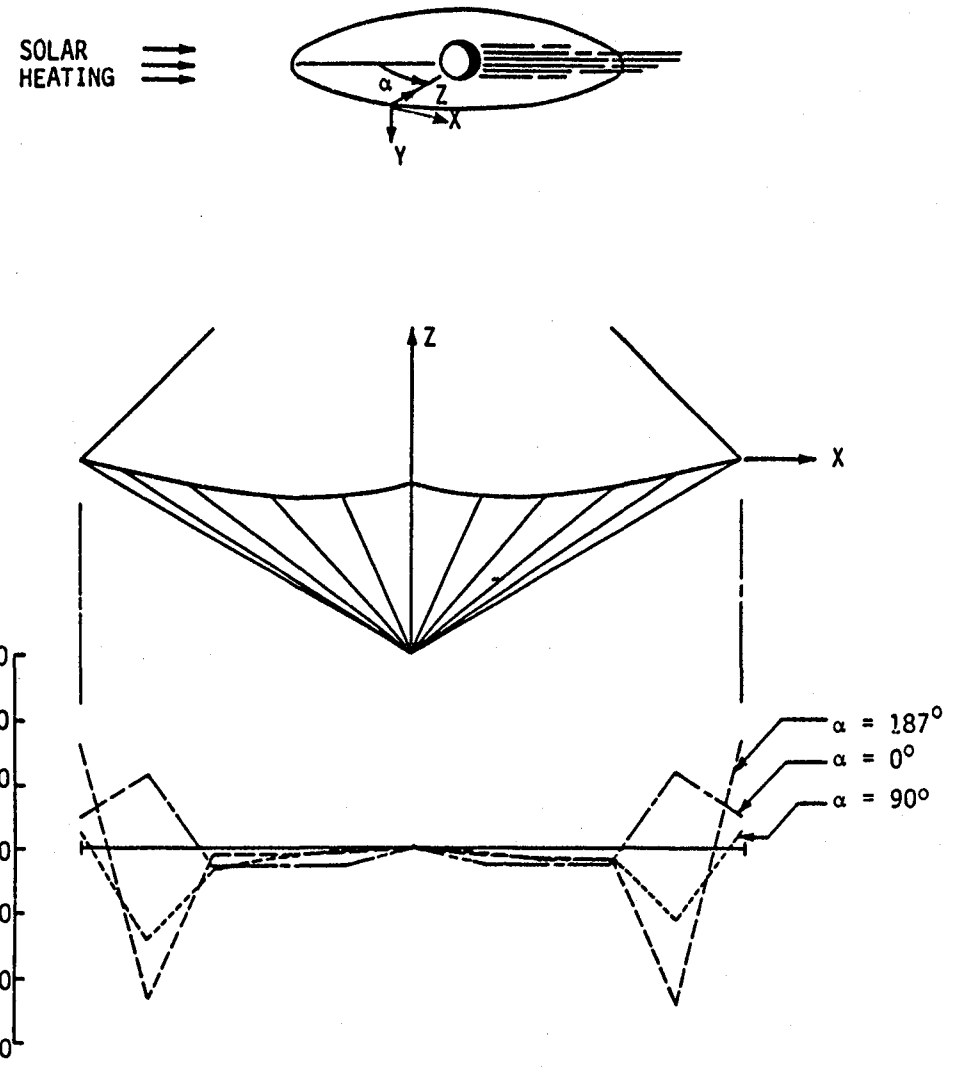

Fig. 30 Displacement distribution at different orbital positions for three-dimensional prestressed hoop column antenna.

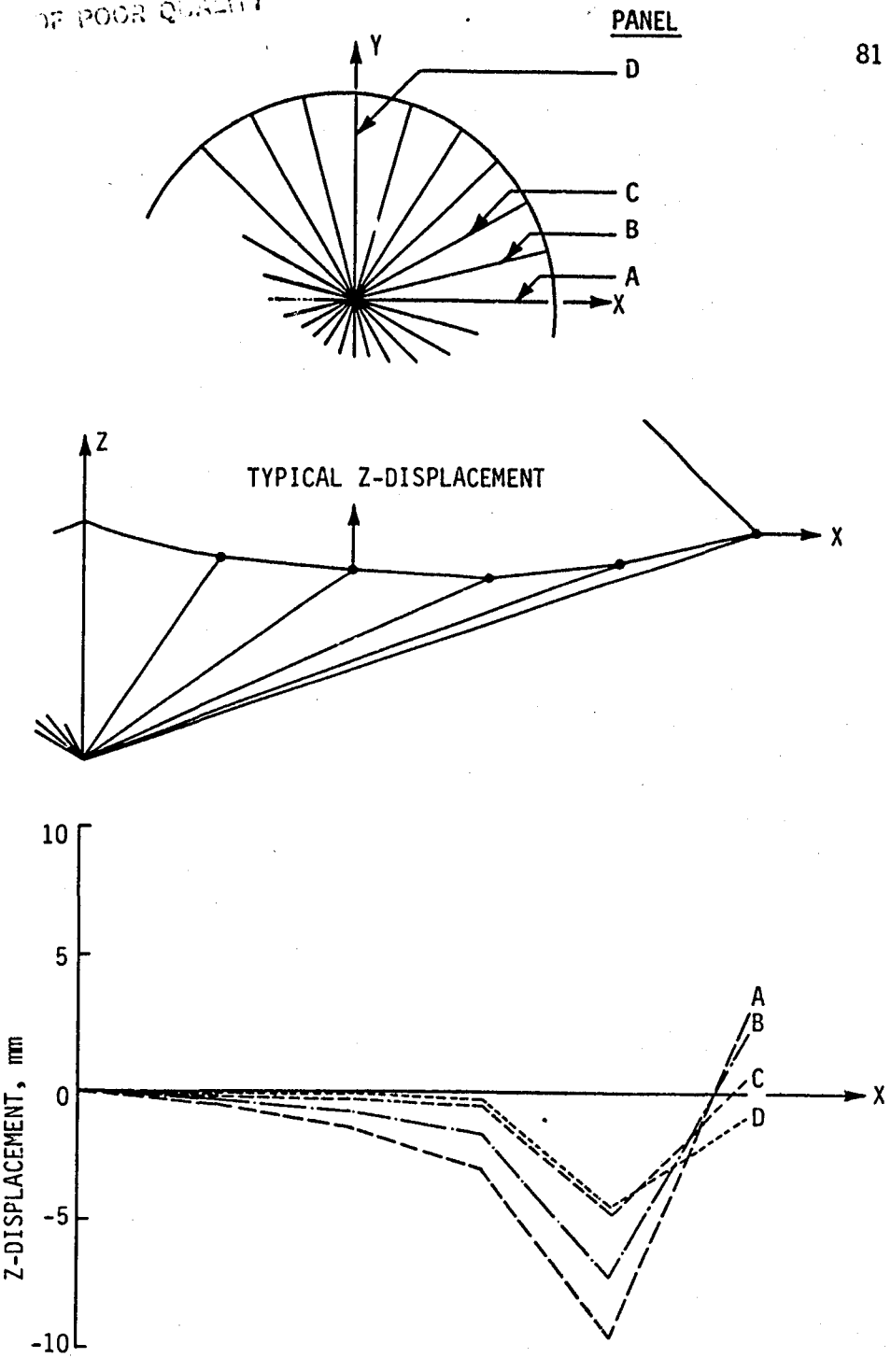

Fig. 31 Displacement of typical panels on antenna surface of prestressed hoop column at 90 degrees orbital position.

A = 10.0 mm
B = 9.0 mm
C = 4.0 mm
D = 0.4 mm
E = 0.3 mm

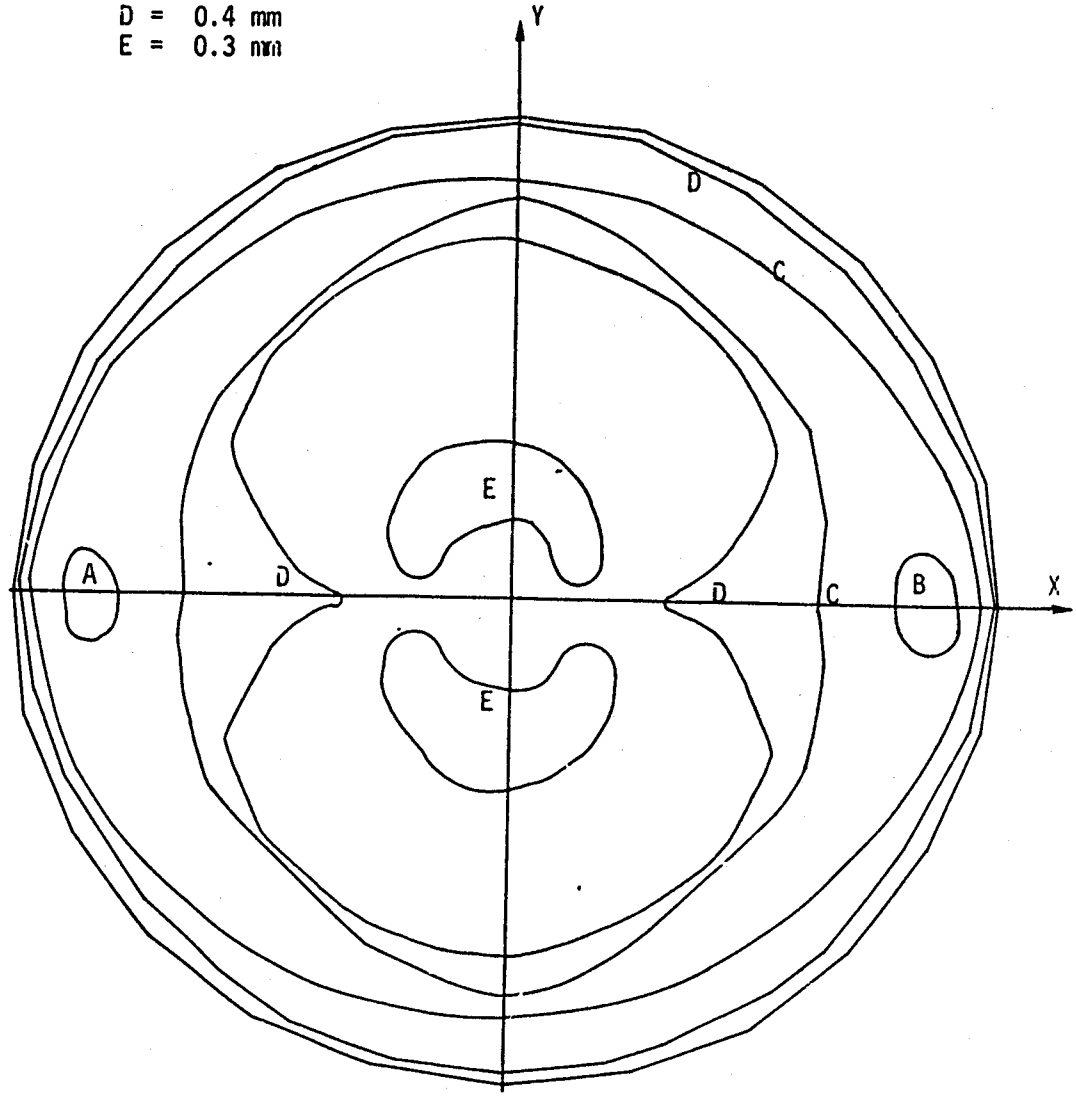

Fig. 32 Approximate displacement contours on antenna surface for hoop column antenna at 90 degrees orbital position.

8.2.3 Comparative Deformations

The linear, stress stiffening and nonlinear structural analyses are performed at three typical prestress levels. Member number five (see Fig. 28) has a force of 226 N for prestress level one, 452 N for prestress level two and 4520 N for prestress level three. The third prestress level is a hypothetical prestress level assumed for evaluation of the three structural analysis techniques. At this prestress some of the members may exceed design allowable stresses in tension or compression. Deflections of a node (number two, Fig. 28) at these prestress levels for the structural analysis techniques are given in Table 6 at 0, 90, and 187 degrees orbital positions.

For all three prestress levels, the linear analysis overestimates the deflection compared to the stress stiffening and nonlinear analyses. With increasing prestress, the linear analysis results remain almost unchanged, but the stress stiffening and nonlinear analysis results change significantly predicting relatively small deflections at higher prestress. In other words, the three analyses produce similar results at small prestress levels, but at higher prestresses the differences between the results from the three techniques becomes greater. For instance, at the zero degree orbital position and at prestress level three, the linear and stress stiffening analysis predict 82 percent and 23 percent higher displacements than the nonlinear analysis.

At NASA design prestresses (level two), results from the three analysis techniques differ significantly. The linear analysis predicts 11 percent, 20.7 percent, and 22.7 percent more deflection than the nonlinear analysis at the three orbital positions. The stress stiffening

Table 6

Prestressed Hoop Column Antenna (Fig. 28)
Z-Deflection Comparison (mm)

ORBITAL POSITION (DEGREES)	0	90	187
PRESTRESS LEVEL ONE (F_S^* = 226.0 N)			
LINEAR ANALYSIS	11.62	-11.40	-24.03
STRESS STIFFENING ANALYSIS	11.31	-10.40	-21.68
NONLINEAR ANALYSIS	10.98	-10.37	-21.66
PRESTRESS LEVEL TWO (F_S = 452.0 N)			
LINEAR ANALYSIS	11.62	-11.40	-24.03
STRESS STIFFENING ANALYSIS	11.01	- 9.49	-19.60
NONLINEAR ANALYSIS	10.45	- 9.44	-19.58
PRESTRESS LEVEL THREE (F_S = 4520.0 N)			
LINEAR ANALYSIS	11.65	-11.37	-24.00
STRESS STIFFENING ANALYSIS	7.89	- 2.15	- 2.97
NONLINEAR ANALYSIS	6.39	- 2.25	- 2.90

*F_S is pretension in member five (see Fig. 28).

analysis predicts 5 percent, 0.5 percent, and 0.1 percent more deflection than the nonlinear analysis at these positions. These results show that at the NASA design prestresses, a stress stiffening analysis can be used instead of a nonlinear analysis to predict deflections with acceptable accuracy.

Comparison of CPU times gives a ratio of 1:11:16 for linear, stress stiffening, and nonlinear analysis, respectively. Although the linear analysis is efficient in computer time, the results of this analysis may not have acceptable accuracy. The nonlinear analysis takes more computer time but the results are always accurate and can be used with confidence for all prestress levels. A stress stiffening analysis is not as expensive as a nonlinear analysis and can give, depending on the prestress, results of acceptable accuracy. Considering these facts the use of the stress stiffening method can be recommended for structural analysis of the hoop column antenna at NASA design prestresses. The nonlinear analysis method is recommended as a more general (and more expensive) technique for all prestress levels.

Chapter 9

CONCLUDING REMARKS

Finite element thermal-structural analysis of cable-stiffened space structures is presented. Heating and thermal analysis for orbiting space structures is first discussed. Determination of cable prestresses is then described. Analysis of structural deformations and stresses are performed using small displacement linear, stress stiffening, and large displacement nonlinear techniques.

To analyze a cable-stiffened space structure, the structural surface heating history is first computed. The thermal analysis is then performed to compute the structural temperature distribution. A prestress analysis is also performed to determine the structural prestresses. The structural temperature distribution and prestresses are used in the structural analysis for computation of deformations and stresses.

To verify the three techniques used in the structural analysis, two examples with analytical solutions are employed. A nonlinear rod-spring system subjected to an external force is first used to assess the accuracy of the three finite element structural analyses. The linear analysis yields a fair result for small deflections. Better accuracy is obtained by using the stress stiffening analysis while the most accurate solution is produced by the large displacement analysis. A cable loaded by its own weight and subjected to a uniform temperature change is used to further verify the accuracy of the large displacement analysis.

C-2

The thermal-structural analysis of a prestressed two-dimensional cable system and a three-dimensional hoop column antenna are performed. The variation of member stress due to thermal effects during the orbit is small compared to the member prestress. The effect of member prestress levels on the accuracy of the analysis techniques is evaluated using comparisons of structural deformations. Finite element analyses for three prestress levels were performed. At low prestresses, the three analysis predict similar deformations. With increasing prestress level, deformations obtained from the linear analysis remain almost unchanged, whereas a large change in deformations is predicted by the stress stiffening and large displacement analyses. Although the linear analysis is efficient in computer time, the results may not have acceptable accuracy. The large displacement analysis takes more computer time, but the results are always accurate and can be used with confidence for all prestress levels. A stress stiffening analysis is not as expensive as a large displacement analysis and it can give, depending on the prestress, results of acceptable accuracy. The stress stiffening method can be recommended for structural analysis of the hoop column antenna at NASA design prestresses.

The large displacement analysis technique is recommended as a general (and more expensive) technique for all prestress levels. The results have shown that accuracy in predicting the deformation and stress for cable stiffened structures strongly depends on the prestress. The large displacement analysis technique produced accurate results over a wide range of prestress and is recommended as a general analysis

approach for thermal-structural analysis of cable-stiffened space structures.

REFERENCES

1. Sullivan, M.R., "LSST (Hoop/Column) Maypole Antenna Development Program," NASA CR-3558, Part 1 & 2, June 1982.

2. Belvin, W.K. "Vibration and Buckling Studies of Pretensioned Structures," Third Annual Technical Review Large Space Systems Technology held at NASA Langley Research Center, Hampton, VA., November 16-22, 1981.

3. Coyner, J.V., Herbert, J.J., and Bachtell, E.E., "15-Meter Diameter Mechanically Scanned Deployable Antenna," NASA CR, April 1982.

4. Huebner, K. and Thornton, E.A., The Finite Element Method for Engineers, Second Edition, John Wiley, 1982.

5. Mahaney, J. and Strode, K.B., "Fundamental Studies of Thermal-Structural Effects on Orbiting Trusses," Proceedings of the AIAA/ASME/ASCE/AHS 23rd Structures, Structural Dynamics and Materials Conference, New Orleans, Louisiana, May 10-12, 1982, AIAA Paper 82-650-CP.

6. Arduini, C., "Model Uncertainties and Approximations in Large Space System Thermal Analysis," International Astronautical Federation, 32nd International Astronautical Congress, Rome, Italy, September 6-12, 1981, IAF Paper 81-376.

7. Chambers B.C., Jensen, C.L. and Coyner, J.V., "An Accurate and Efficient Method for Thermal/Thermoelastic Performance Analysis of Large Space Structures," AIAA 16th Thermophysic Conference, Palo Alto, CA., June 23-25, 1981.

8. Thornton, E.A., Dechaumphai, P. and Wieting, A.R., "Integrated Finite Element Thermal-Structural Analysis with Radiation Heat Transfer," Proceedings of the AIAA/ASME/ASCE/AHS 23rd Structures, Structural Dynamics and Materials Conference, New Orleans, Louisiana, May 10-12, 1982, AIAA Paper 82-0703.

9. Bowles, D.E. and Tenney, D.R., "Thermal Expansion of Composites: Methods and Results," Second Annual Technical Review Large Space Systems Technology held at NASA Langley Research Center, Hampton, VA., November 18-20, 1980, NASA CP-2168, Part 1, pp. 119-128.

10. Cox, R.H., "Report on the Design Phase of the Cable Boom Development Study," European Space Research Organization, October 1972.

11. Pearson, J., "Lunar Anchored Satellite Test," Proceedings of the AIAA/AAS Astrodynamics Conference, Palo Alto, CA., August 7-9, 1978, AIAA Paper 78-1427.

12. Sumberg, R.E., "The Geosynchronous Tidal Web, A Method for Constructing an Ultra-Large Space Structure," Proceedings of the Fifth Princeton/AIAA Conference, May 18-21, 1981.

13. Clarke, A.C., "The Space Elevator: 'Thought Experiment,' or Key to the Universe," Advances in Earth Oriented Applications of Space Technology, Vol. 1, No. 1, 1981.

14. Conaway, A.E., "A Comparison of Linear and Geometrically Nonlinear Finite Element Analyses Applied to Large Space Structures," AIAA 22nd Aerospace Science Meeting, January 9-12, 1984, Reno, Nevada.

15. Irvine, H.M., Cable Structures, The MIT Press, 1981.

16. Baron, F. and Venkatesan, M.S., "Nonlinear Analysis of Cable and Truss Structures," Journal of the Structural Division, Proceedings of ASCE, February 1971.

17. "ANSYS Reference Manual," Section 2.22 and 2.23, Swanson Analysis Systems, Inc., Houston, PA.

18. Cook, R.D., Concepts and Applications of Finite Element Analysis," John Wiley, 1974.

19. Carnahan, B., Luther, H.A. and Wilkes, J.O., Applied Numerical Methods, John Wiley, 1969.

20. Stricklin, J.A., Haisler, W.E. and Riesemann, W.A., "Geometrically Nonlinear Structural Analysis By Direct Stiffness Method," Journal of Structural Division, Proceedings of ASCE, Vol. No. 1, September 1971.

APPENDICES

APPENDIX A

FINITE ELEMENT MATRICES FOR STRESS STIFFENING STRUCTURAL ANALYSIS

The finite element equations shown in Eqs. (5.5) for the stress stiffening structural analysis have the form,

$$\frac{AE}{L}[\bar{K}]\begin{Bmatrix} u_1 \\ v_1 \\ w_1 \\ u_2 \\ v_2 \\ w_2 \end{Bmatrix} = AE\alpha\,(T-T_i)\begin{Bmatrix} -1 \\ 0 \\ 0 \\ 1 \\ 0 \\ 0 \end{Bmatrix} + A\sigma_0\begin{Bmatrix} 1 \\ 0 \\ 0 \\ -1 \\ 0 \\ 0 \end{Bmatrix} + \begin{Bmatrix} P_1 \\ 0 \\ 0 \\ P_2 \\ 0 \\ 0 \end{Bmatrix} \qquad (A.1)$$

where $[\bar{K}]$ is a symmetric matrix in which the coefficients are,

$$\begin{aligned}
\bar{K}_{11} &= -\bar{K}_{14} = \bar{K}_{44} = 1 \\
\bar{K}_{12} &= -\bar{K}_{15} = \bar{K}_{45} = \frac{\theta}{2} \\
\bar{K}_{13} &= -\bar{K}_{16} = \bar{K}_{46} = \frac{\psi}{2} \\
\bar{K}_{22} &= -\bar{K}_{25} = \bar{K}_{55} = \frac{1}{2}\left[\alpha\,(T-T_i) + \frac{\sigma_0}{E} + \frac{\theta^2}{2}\right] \\
\bar{K}_{23} &= -\bar{K}_{26} = \bar{K}_{56} = \frac{\theta\psi}{4} \\
\bar{K}_{33} &= -\bar{K}_{36} = \bar{K}_{66} = \frac{1}{2}\left[\alpha\,(T-T_i) + \frac{\sigma_0}{E} + \frac{\psi^2}{2}\right]
\end{aligned} \qquad (A.2)$$

$$\bar{K}_{34} = -\frac{\psi}{2}$$

$$\bar{K}_{35} = -\frac{\theta\psi}{4}$$

The first term on the right-hand side of the above equation denotes the element nodal force vector associated with the thermal load. Isothermal elements were used in the thermal analysis so the element temperature T is constant for the element.

APPENDIX B

FINITE ELEMENT MATRICES FOR LARGE DEFLECTION STRUCTURAL ANALYSIS

Components of the element matrices shown in Eqs. (6.5) are presented here. The element equations can be written in the form,

$$\frac{AE}{L}[\bar{J}]\begin{Bmatrix}\Delta u_1\\ \Delta v_1\\ \Delta w_1\\ \Delta u_2\\ \Delta v_2\\ \Delta w_2\end{Bmatrix} = AE\alpha\,(T-T_i)\begin{Bmatrix}-1\\0\\0\\1\\0\\0\end{Bmatrix} + A\sigma_0\begin{Bmatrix}e\\0\\0\\-e\\0\\0\end{Bmatrix} + \begin{Bmatrix}R_1\\R_2\\R_3\\R_4\\R_5\\R_6\end{Bmatrix}_{\theta,\psi} + \begin{Bmatrix}P_1\\0\\0\\P_2\\0\\0\end{Bmatrix} \qquad (B.1)$$

where components of symmetric matrix $[\bar{J}]$ are given by

$$\begin{aligned}
\bar{J}_{11} &= -\bar{J}_{14} = \bar{J}_{44} = 1\\
\bar{J}_{12} &= -\bar{J}_{15} = \bar{J}_{45} = -\bar{J}_{24} = \theta\\
\bar{J}_{13} &= -\bar{J}_{16} = \bar{J}_{46} = -\bar{J}_{34} = \psi\\
\bar{J}_{22} &= -\bar{J}_{25} = \bar{J}_{55} = \left[e - \alpha\,(T-T_i) + \frac{\sigma_0}{E} + \frac{3}{2}\theta^2 + \frac{\psi^2}{2}\right] \qquad (B.2)\\
\bar{J}_{23} &= -\bar{J}_{26} = \bar{J}_{56} = \theta\psi\\
\bar{J}_{33} &= \bar{J}_{66} = \left[e - \alpha\,(T-T_i) + \frac{\sigma_0}{E} + \frac{3}{2}\psi^2 + \frac{\theta^2}{2}\right]
\end{aligned}$$

The fourth vector on the right-hand side of the above equation is asso-

ciated with the rotational strain and the components are given by,

$$R_1 = -R_4 = \frac{\theta^2}{2} + \frac{\psi^2}{2}$$

$$R_2 = -R_5 = \left[e - \alpha\,(T-T_i) + \frac{\sigma_0}{E}\right]\theta + \frac{\theta^3}{2} + \frac{\theta\psi^2}{2}$$

$$R_3 = -R_6 = \left[e - \alpha\,(T-T_i) + \frac{\sigma_0}{E}\right]\psi + \frac{\psi^3}{2} + \frac{\psi\theta^2}{2}$$

Thermal strain terms in the above equations have been replaced by Eq. (4.7). Isothermal elements were used in the thermal analysis so the element temperature T is constant for the element.

END

DATE

FILMED

SEP 26 1984